AD-A089 412 GEORGIA INST OF TECH ATLANTA ENGINEERING EXPERIMENT --ETC F/G 20/3
ANALYSIS AND MEASUREMENTS OF THREE-DIMENSIONAL ARBITRARILY-SHAP--ETC(U)
MAY 80 J J WANG, C PAPANICOLOPULOS F19628-78-C-0223
UNCLASSIFIED RADC-TR-80-167 NL

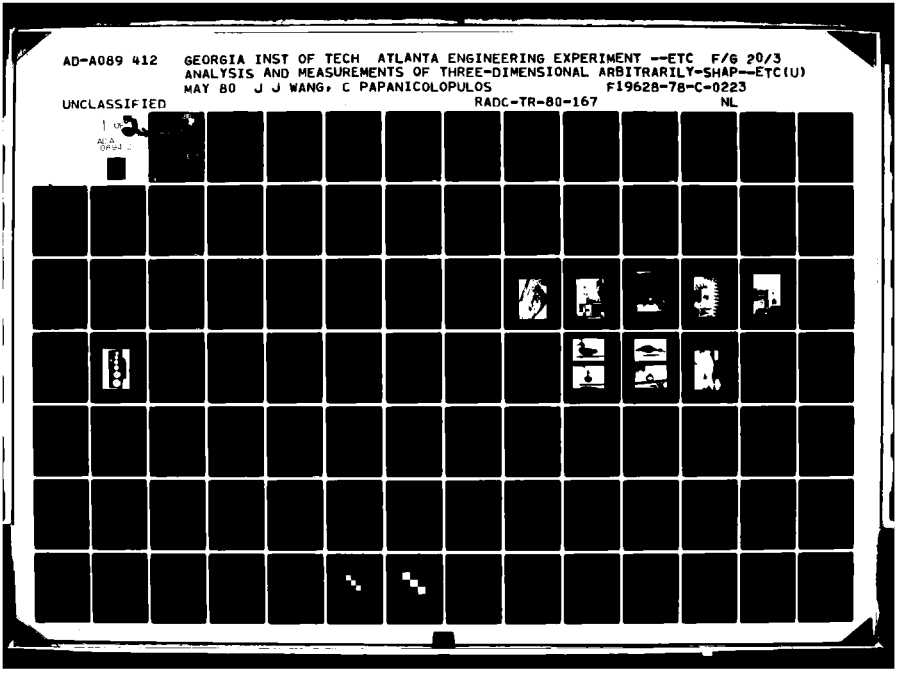

(12) LEVEL II

RADC-TR-80-167
Interim Report
May 1980

ANALYSIS AND MEASUREMENTS OF THREE-DIMENSIONAL ARBITRARILY-SHAPED DIELECTRIC SCATTERERS

Georgia Institute of Technology

J. J. H. Wang
C. Papanicolopulos

ROME AIR DEVELOPMENT CENTER
Air Force Systems Command
Griffiss Air Force Base, New York 13441

AIR FORCE (1)--AUGUST 7, 1980--163

This report has been reviewed by the RADC Public Affairs Office (PA) and is releasable to the National Technical Information Center (NTIS). At NTIS it will be releasable to the general public, including foreign nations.

RADC-TR-80-167 has been reviewed and is approved for publication.

APPROVED: Otho E. Kerr

OTHO E. KERR
Project Engineer

APPROVED:

ALLAN C. SCHELL
Chief, Electromagnetic Sciences Division

FOR THE COMMANDER: John P. Huss

JOHN P. HUSS
Acting Chief, Plans Office

If your address has changed or if you wish to be removed from the RADC mailing list, or if the addressee is no longer employed by your organization, please notify RADC (EEC), Hanscom AFB MA 01731. This will assist us in maintaining a current mailing list.

Do not return this copy. Retain or destroy.

UNCLASSIFIED

SECURITY CLASSIFICATION OF THIS PAGE (When Data Entered)

REPORT DOCUMENTATION PAGE

READ INSTRUCTIONS BEFORE COMPLETING FORM

1. REPORT NUMBER: RADC-TR-80-167	2. GOVT ACCESSION NO.: AD-A089412
3. RECIPIENT'S CATALOG NUMBER:	
4. TITLE (and Subtitle): ANALYSIS AND MEASUREMENTS OF THREE-DIMENSIONAL ARBITRARILY-SHAPED DIELECTRIC SCATTERERS.	5. TYPE OF REPORT & PERIOD COVERED: Interim Report - Sep 78 — Jan 80
	6. PERFORMING ORG. REPORT NUMBER: N/A
7. AUTHOR(s): J. J. H. Wang; C. Papanicolopulos	8. CONTRACT OR GRANT NUMBER(s): F19628-78-C-0223
9. PERFORMING ORGANIZATION NAME AND ADDRESS: Georgia Institute of Technology, Engineering Experiment Station, Atlanta GA 30332	10. PROGRAM ELEMENT, PROJECT, TASK AREA & WORK UNIT NUMBERS: 61102F; 2305J437
11. CONTROLLING OFFICE NAME AND ADDRESS: Deputy for Electronic Technology (RADC/EEC), Hanscom AFB MA 01731	12. REPORT DATE: May 1980; 13. NUMBER OF PAGES: 102
14. MONITORING AGENCY NAME & ADDRESS (if different from Controlling Office): Same	15. SECURITY CLASS. (of this report): UNCLASSIFIED; 15a. DECLASSIFICATION/DOWNGRADING SCHEDULE: N/A

16. DISTRIBUTION STATEMENT (of this Report)

Approved for public release; distribution unlimited.

17. DISTRIBUTION STATEMENT (of the abstract entered in Block 20, if different from Report)

Same

18. SUPPLEMENTARY NOTES

RADC Project Engineer: Otho E. Kerr (RADC/EEC)

19. KEY WORDS (Continue on reverse side if necessary and identify by block number)

Method of Moments
Arbitrarily-shaped Dielectric Scatterers
Electromagnetic Scattering and Radiation
Integral Equation Solution
Dyadic Green's Function

20. ABSTRACT (Continue on reverse side if necessary and identify by block number)

Theoretical and experimental research was conducted to determine the electromagnetic scattering from heterogeneous dielectric bodies. The discrepancies in the literature regarding the singularity of the electric dyadic Green's functions were resolved. Compact range scattering measurements at 1 GHz were successfully performed. Extensive computations were made for a variety of dielectric scatterers, including a one-foot bird at 1 GHz. The agreements between measurements and

DD FORM 1 JAN 73 1473 EDITION OF 1 NOV 65 IS OBSOLETE

UNCLASSIFIED (Cont'd)

SECURITY CLASSIFICATION OF THIS PAGE (When Data Entered)

153850

Item 20 (Cont'd)

computation were good except for the resonant sphere, for which the calculated resonant frequencies were shifted by about 20 percent. Various numerical techniques, to treat symmetrical scatterers, using symmetric matrices, banded matrices, and virtual memory were implemented in the Volume Integral Equation algorithm.

SUMMARY

The objective of this program is to conduct theoretical and experimental research to determine the electromagnetic scattering from heterogeneous dielectric bodies as individual bodies and as a cluster of bodies. The discrepancies in the literature regarding the singularity of the electric dyadic Green's functions were resolved. Compact range scattering measurements at 1 GHz were successfully performed to obtain measured data to validate the numerical analyses. Extensive computations were made for a variety of dielectric scatterers, including a one-foot bird at 1 GHz. The agreements between measurement and computation were good except for the resonant sphere, for which the calculated resonant frequencies were shifted by about 20 percent. Various numerical techniques were investigated successfully for implementation in the volume integral equation algorithm at Georgia Tech. These techniques include methods to treat symmetrical scatterers through use of symmetric matrices, and the use of banded matrices, and virtual memory.

There has been very little research into the problem of scattering by dielectric objects of complex permittivity. Future research in this area should include the investigation of the surface integral equation technique and the exact solution for the dielectric prolate spheroid.

PREFACE

The research on this contract was carried out in the Electromagnetic Effectiveness Division of the Electronics Technology Laboratory of the Engineering Experiment Station at the Georgia Institute of Technology, Atlanta, Georgia 30332. Dr. Johnson J. Wang served as the Project Director. This program is sponsored by the Rome Air Development Center, Air Force Systems Command and was designated on Georgia Tech Project A-2212. This interim report covers the work which was performed from 1 September 1978 to 31 January 1980.

The authors wish to express their gratitude to Mr. Otho E. Kerr, Drs. John K. Schindler and Lee Poirier for their interest and support in this research. The authors also acknowledge the various contributions in the compact-range scattering measurements by Messrs. E. E. Weaver, W. P. Cooke, F. L. Cain and Dr. C. E. Ryan, Jr.

Respectfully submitted,

Johnson J. Wang
Project Director

Approved:

Charles E. Ryan, Jr.
Chief,
EM Effectiveness Division

TABLE OF CONTENTS

TABLE OF CONTENTS (Continued)

LIST OF FIGURES

LIST OF FIGURES (Continued)

LIST OF FIGURES (Continued

LIST OF TABLES

SECTION I
INTRODUCTION

During the past decade, there has been a rapidly rising interest in electromagnetic problems involving dielectric objects. The interest in this area arises from a multitude of military and civilian needs. Human beings are increasingly more exposed to microwave radiation hazards on aircraft, ships, military installations and even in their homes. The electromagnetic scattering from birds, animals, and human beings is essential to the detection, identification, and interference problems in radar systems. Biological and medical applications, such as blood thawing, enzyme inactivation and hyperthermia treatment of cancerous tissues, also demand accurate knowledge of the electromagnetic fields in dielectric bodies. Thus, electromagnetic scattering by dielectric bodies is a fundamental and important problem, and solutions for these scatterers have wide application.

Since September 1978, Georgia Tech has been supported by the Deputy for Electronic Technology (RADC/EEC), Air Force Systems Command, under contract F19628-78-C-0223 to conduct a two-year research program in this area. The emphasis is focused on analyses and measurements of the scattering characteristics of heterogeneous dielectric objects as individual bodies and as a cluster of bodies. Progress to date has included the clarification of discrepancies in the literature on the singularity of the Green's function in the source region [1], and measurements and calculations of the scattering cross-section of dielectric bodies of arbitrary shapes and complex dielectric constants [2-4]. In addition, various numerical techniques have been investigated and implemented in the existing Volume Integral Equation (VIE) algorithm at Georgia Tech.

Numerical techniques developed in the current research program are capable of producing fairly accurate data for objects less than one free-space wavelength long. There are models for which the present technique is highly accurate, and there are geometries, such as the sphere, for which the present technique is not quite satisfactory.

The success of compact-range scattering measurements at a frequency of 1 GHz represents an advance in the state-of-the-art of scattering measurements using the compact range technique. This extension of the compact range scattering measurements to lower frequencies demonstrates the versatility and usefulness of the compact range as a general purpose EM measurements facility.

SECTION II

RESOLUTION OF THE DISCREPANCIES IN THE SINGULARITIES OF THE ELECTRIC DYADIC GREEN'S FUNCTIONS

Green's functions of various types are fundamental to the theory of electromagnetics and have become increasingly important with the recent progress in numerical analysis. The dyadic Green's function technique of treating electromagnetic boundary-value problems was first formulated by Schwinger in the early 1940's in unpublished notes. This subject was described in several textbooks by Morse and Feshbach [5], Collin [6], Schwinger and Saxon [7], and Tai [8]. Recently, the usefulness of Green's functions in electromagnetic theory increased due to the use of high-speed computers to numerically analyze many problems previously unsolvable. Computerized analysis often employs an integral equation [9] which evolves from a Green's function expression for the particular boundary conditions. However, earlier Green's function expressions have been limited to the space outside the source region and are deficient when used in the integral equation formulations. This deficiency was addressed with an increasing interest in recent literature [1,5,8,10-23]. However, some of the results in the literature appear to be inconsistent [14,17,19-21] with seemingly conflicting results.

Yaghjian attempted to explain the apparent discrepancy in the singularities of electric dyadic Green's functions as due to the differences in the shape of the principal volumes involved in the formulations [19-21]. Unfortunately, the principal volume was apparently not involved at all in the derivation of the controversial expressions [14,17].

In this section, the source singularity of the electric dyadic Green's function will be discussed and a more satisfactory view on this subject will be presented. The authors concur with Yaghjian in that the singularity of the electric dyadic Green's functions does depend on the principal volume selected. However, we do not share his view on the necessity or even correctness of attaching the principal volume to the electric dyadic Green's function. The principal volume integration is merely a mathematical

process taken to deal with the singularity of the electric dyadic Green's function in the source region. In fact, it may be possible to select a finite volume to handle the integration without resorting to the principal volume [23], which must be infinitely small and of a specific shape . The apparent discrepancy between Tai and Rozenfeld [14] and Yaghjian [15] has been found to be non-existent and their expressions are mathematically identical.

A. The Apparent Discrepancies in the Source Singularity of the Electric Dyadic Green's Functions

A dyadic Green's function has been conventionally defined for a time-harmonic field in either of the following two ways.

1. Method of Delta Function or Distribution Theory

The dyadic Green's function can be defined [8] as a dyad $\underline{\underline{G}}(\underline{r},\underline{r}')$ that satisfies the complex vector wave equation

$$\nabla \times \nabla \times \underline{\underline{G}}(\underline{r},\underline{r}') - k^2 \underline{\underline{G}}(\underline{r},\underline{r}') = \underline{\underline{I}}\, \delta\, (\underline{r},\underline{r}'), \tag{1}$$

subject to all the boundary conditions, where

∇ = gradient operator,
k = the wavenumber of the medium,
$\underline{\underline{I}}$ = unit dyad,
δ = Dirac delta function, and
$\underline{r},\underline{r}'$ = positional vectors of the field and source points, respectively.

The problem is illustrated in Figure 1. This definition was used in References 5,7,8,13,14,16 and 17.

2. The Integral Formula Method

The dyadic Green's function is defined, in the integral formula method [24], as a dyad $\underline{\underline{G}}(\underline{r},\underline{r}')$ that satisfies

$$\underline{E}(\underline{r}) = - \int_V \underline{\underline{G}}(\underline{r},\underline{r}') \cdot \underline{J}(\underline{r}')\, dv' \tag{2}$$

where $\underline{E}$ is the electric field and $\underline{J}$ is the electric current.

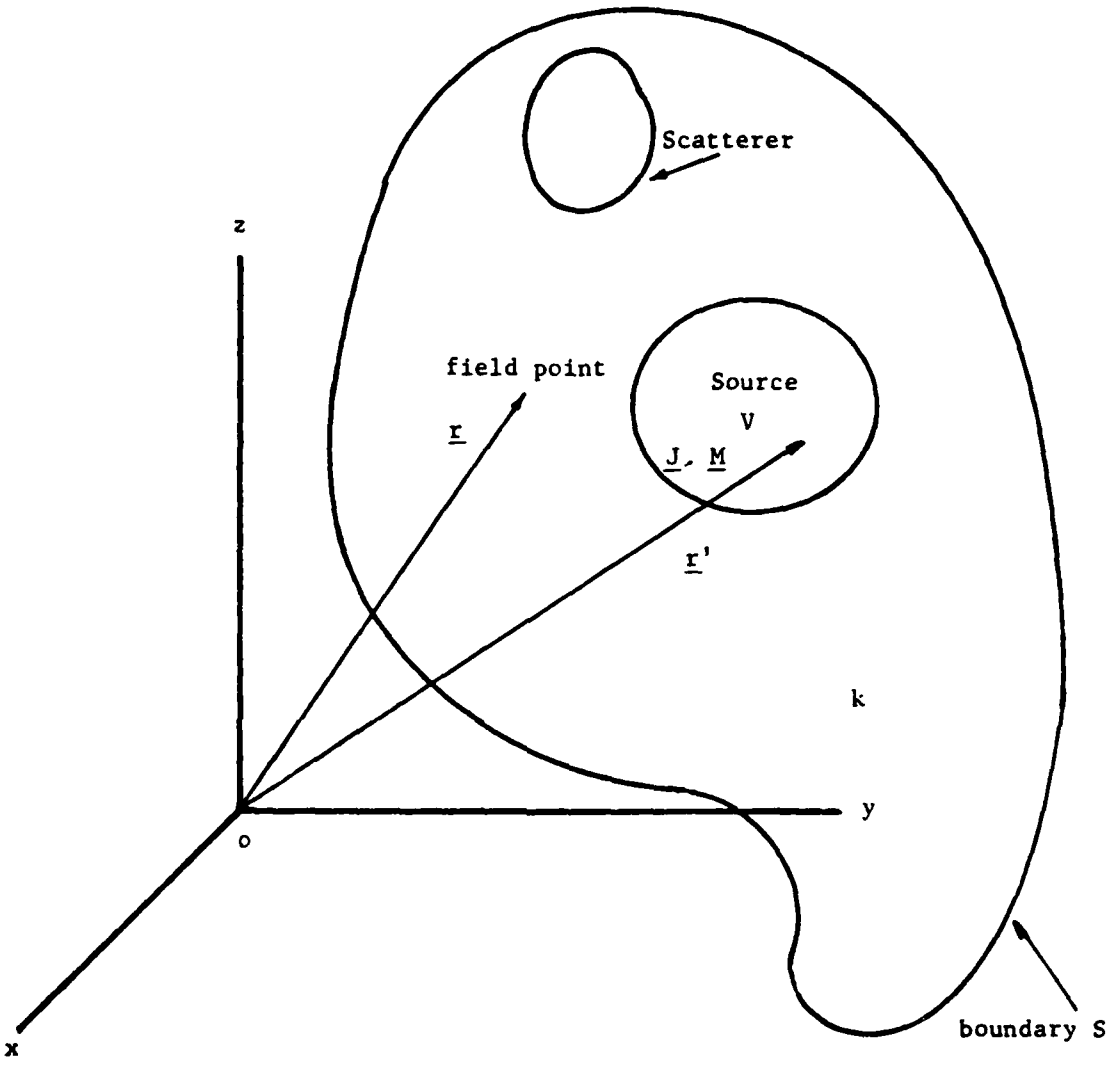

Figure 1. A general electromagnetic boundary-value problem.

The singular behavior of the dyadic Green's functions can be best illustrated by its simplest type -- the free-space electric type, for which

$$\underline{\underline{G}}_o(\underline{r},\underline{r}') = j\omega\mu_o[\underline{\underline{I}} + \frac{\nabla\nabla}{k^2}] \frac{e^{-jk|\underline{r} - \underline{r}'|}}{4\pi|\underline{r} - \underline{r}'|} . \tag{3}$$

As $\underline{r} \to \underline{r}'$, the denominator in Equation (3) vanishes and $\underline{\underline{G}}_o$ is singular at this point. However, when $\underline{\underline{G}}_o$ is used in an integral formulation, the resulting integral is expected to yield a finite value. This problem is well known to the mathematicians and has been discussed by Van Bladel [12] with respect to electromagnetic theory. As shown in Figure 2, Van Bladel placed an infinitesimal volume ΔV, surrounded by a closed surface ΔS, to enclose the field point $\underline{r}'$which is located in the source region. The electric field was then expressed as

$$\underline{E}(\underline{r}) = \int_{V - \Delta V} \underline{\underline{G}}_o(\underline{r},\underline{r}') \cdot \underline{J}(\underline{r}')\, dv' + \int_{\Delta V} \underline{\underline{G}}_o(\underline{r},\underline{r}') \cdot \underline{J}(\underline{r}')\, dv'$$

$$\equiv \int_{V - \Delta V} \underline{\underline{G}}_o(\underline{r},\underline{r}') \cdot \underline{J}(\underline{r}')\, dv' + \underline{E}_c(\underline{r}) \tag{4}$$

in which $\underline{E}_c$, the correction term, was employed to account for the removal of ΔV from the integral, and $\int_{V-\Delta V}$ was referred to as the "principal volume" integration. The $\underline{E}_c$ term was not clearly spelled out in Van Bladel's work, but was later employed by Chen [14] to provide a clearer picture of the physics involved and this notation is convenient for the present discussion.

Van Bladel noted that $\underline{E}_c(\underline{r})$ does not converge properly if ΔS is a circular cylinder, but he found that

$$\underline{E}_c(\underline{r}) = \frac{-\underline{J}(\underline{r})}{j3\omega\varepsilon_o} \tag{5}$$

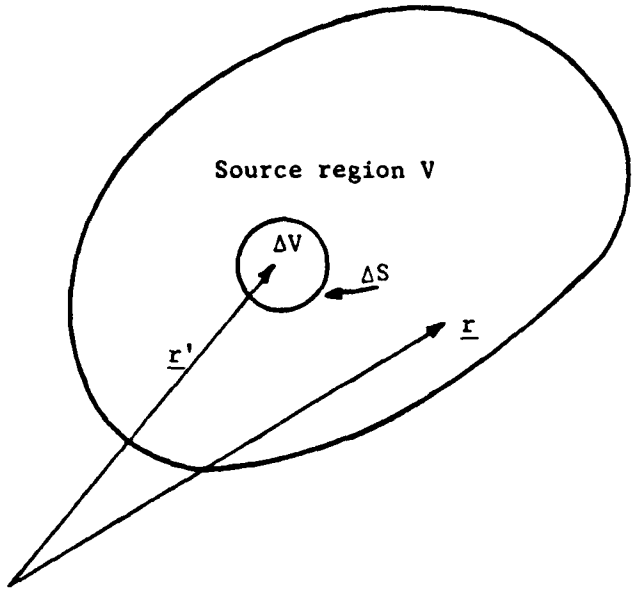

Figure 2. "Principal Volume" integration in the source region.

if ΔS is chosen to be a sphere. Equation (5), based on a spherical ΔS, was employed successfully in numerical analysis in both References 25 and 26.

Recently, Yaghjian [19-21] pointed out the apparent discrepancies in the literature when other types of dyadic Green's functions and infinitesimal volumes ΔV were involved. Rahmat-Samii [17] showed that

$$\underline{E}_c = \frac{-\underline{J}}{j\omega\varepsilon_o} \quad , \tag{6}$$

for a rectangular cavity without specifying the principal volume, if any, being involved. For the same problem, Tai and Rozenfeld [14] indicated

$$\underline{E}_c = \frac{-J_z \hat{z}}{j\omega\varepsilon_o} \quad , \tag{7}$$

without specifying the principal volume.

Apparently in an effort to resolve the discrepancy between Equations (6) and (7), Yaghjian [19-21] carried out an analysis to demonstrate that $\underline{E}_c$ depends on the choice of the shape for the infinitesimal volume ΔV. Furthermore, he states that the same is true for problems involving boundary surfaces on which tangential $\underline{E}$ or $\underline{B}$ are zero. Unfortunately, his reported results introduced several more discrepancies which added more confusion in spite of his intended effort to unify and to interpret. For example, in the rectangular cavity case, Yaghjian offered the following answer

$$\underline{E}_c = \frac{\underline{J}}{j3\omega\varepsilon_o} \qquad \text{if } \Delta V \text{ is a cube,} \tag{8a}$$

$$\underline{E}_c = \frac{J_z \hat{z}}{j\omega\varepsilon_o} \qquad \text{if } \Delta V \text{ is a pillbox .} \tag{8b}$$

While Equation (8b) is similar to Equation (7), Equation (8a) differs from both Equations (6) and (7). The differences in sign are due to their differences in the suppressed $e^{j\omega t}$ or $e^{-j\omega t}$ chosen in the individual analyses; they can be ignored.

Chen [18] indicated the dependence on the shape of the principal volume but restricted his discussion to the free space case only. However, his expression for a circular cylinder ΔV is, by assuming $\underline{J} = \hat{z}J_z$,

$$\underline{E}_c = \frac{-\underline{J}}{j\omega\varepsilon_o} \quad (1 - \cos\theta_o) \tag{9}$$

while Yaghjian's formula is

$$\underline{E}_c = [(1 - \cos\theta_o) \quad J_z\hat{z} + 1/2 \cos\theta_o \underline{J}] \quad \frac{-1}{j\omega\varepsilon_o} \tag{10}$$

where θ_o is shown in Figure 3.

The discrepancies in the literature as discussed above are partially summarized in Table 1 for ready comparison. As can be seen, no major disagreement exists in the literature for the free space case. But for the rectangular cavity and waveguide, there are apparent discrepancies among various authors.

B. The Uniqueness of a Harmonic Field

The uniqueness theorem for a harmonic field is stated by Harrington [27] as:

"A field in a lossy region is uniquely specified by the sources within the region plus the tangential components of $\underline{E}$ over the boundary, or the tangential $\underline{H}$ over the boundary, or the former over part of the boundary and the latter over the rest of the boundary".

A similar form of the uniqueness theorem was stated by Richmond [28] as:

"In a region completely occupied with dissipative media, a harmonic field is determined uniquely by the impressed currents in the region and the tangential components of the electric or magnetic field intensity on the surface of the region".

Note that Richmond's version is more stringent in that the region must be "completely" filled with "dissipative" media. Although these two conditions for the theorem appear to be severe restrictions, one can

TABLE 1

DISCREPANCIES IN $\underline{E}_c(-j\omega\epsilon_o)$ IN THE LITERATURE

Boundary	Principal Volume ΔV*	Yaghjian	Chen	Tai	Rahmat-Samii	Collin
Free Space	Sphere	$\underline{J}/3$	$\underline{J}/3$			
	Circular Cylinder	$(1-\cos\theta_o)J_z\hat{z}$ $+1/2\ \cos\theta_o\underline{J}$	$(1-\cos\theta_o)\underline{J}$			
	Cube	$\underline{J}/3$	$\underline{J}/3$			
Rectangular Cavity	Cube	$\underline{J}/3$		$J_z\hat{z}$	$\underline{J}$	
	Pill Box	$J_z\hat{z}$				
Rectangular Waveguide	Cube	$\underline{J}/3$		$J_z\hat{z}$	$J_z\hat{z}$	$J_z\hat{z}$
	Pill Box	$J_z\hat{z}$				

* See Figure 3.

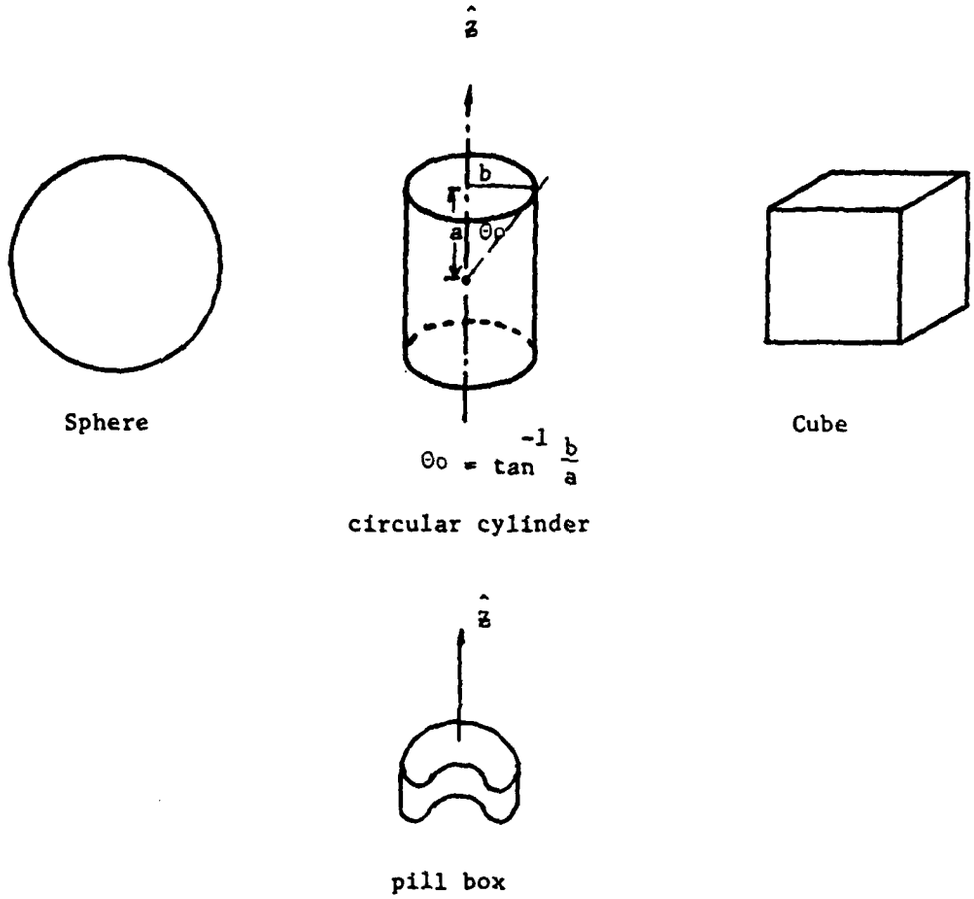

Figure 3. Various Shapes of ΔV for the Calculation of principal-volume integration.

practically apply this theorem to almost any physical problem. It can be stated from the viewpoint of atomic physics, that all the space is filled with energy and material, which are "lossy" because of the necessary transfer of energy involved between the field and the media. The purely conducting and lossless medium does not exist in reality, at least not in the electromagnetic problems known to the authors.

In order to extend the uniqueness theorem to a lossless medium, Harrington [27] indicated that "We (can) consider the field in a dissipationless medium to be the limit of the corresponding field in a lossy medium as the dissipation goes to zero". This limiting process does not add to the usefulness of the uniqueness theorem. In fact, the method is not strictly correct since there <u>are</u> two or more possible solutions for lossless media. Examples are the field inside a perfectly conducting spherical shell illuminated by a plane wave and the surface waves involved in scattering by a lossless dielectric slab of finite thickness and infinite width under the excitation of a plane wave. Therefore, one cannot use this limiting process to obtain the approximate solution for a slightly lossy medium from a solution derived from a lossless medium.

C. The Uniqueness of Green's Functions

The uniqueness of Green's functions can be proved based on their integral-formula definition of Equation (2). Assume that there are two Green's functions $\underline{\underline{G}}^1$ and $\underline{\underline{G}}^2$ for a specific boundary-value problem for which the excitation and field are unique, we have

$$\underline{E}(\underline{r}) = \int_V \underline{\underline{G}}^1(\underline{r},\underline{r}') \cdot \underline{J}(\underline{r}')\, dv', \tag{11}$$

and

$$\underline{E}(\underline{r}) = \int_V \underline{\underline{G}}^2(\underline{r},\underline{r}') \cdot \underline{J}(\underline{r}')\, dv'. \tag{12}$$

Since $\underline{J}(\underline{r}')$ is arbitrary, we can choose

$$\underline{J}(\underline{r}') = \hat{e}\,\delta\,(\underline{r}-\underline{r}'). \tag{13}$$

Subtractions between Equations (11) and (12) and substitution of Equation (13) yield

$$\hat{e} \cdot [\underline{\underline{G}}^1(\underline{r},\underline{r}') - \underline{\underline{G}}^2(\underline{r},\underline{r}')] = 0 \tag{14}$$

Hence

$$\underline{\underline{G}}^1(\underline{r},\underline{r}') = \underline{\underline{G}}^2(\underline{r},\underline{r}') \tag{15}$$

This completes the proof for the uniqueness of the Green's function. Note that the uniqueness of the fields is essential to this proof.

D. The Singularity of the Electric Dyadic Green's Function in the Source Region

The field $\underline{E}_c$ at a singular point as defined in Equation (4) is, in general, dependent upon the infinitismal volume ΔV. The integral over $V-\Delta V$ in Equation (4) is also generally dependent on ΔV so that the total field $\underline{E}(\underline{r})$ is uniquely determined at $\underline{r}$. In fact, the problem of determining the integral over $V-\Delta V$ is as important as the problem of "extracting" the singularity. Merely extracting a term containing a Dirac-delta function does not necessarily lead to the extraction of the singularity.

Yaghjian [19-21] apparently overemphasized the importance of the principal volume and considered it a part of the definition for the Green's function in the source region. Lee and Law [23] showed that ΔV in Equation (4) need not be small and can be finite and of arbitrary shape. As a result of our investigation, it is shown that a unique Green's function exists and thus there is no need for a new definition for the electric dyadic Green's function. The significance of Yaghjian's work is his correct emphasis on the shape of the principal volume which affects both the integrals over ΔV and $V-\Delta V$. In dealing with the singularity in the source

region, the importance of handling the integral over V-ΔV has been recognized when one actually computes the field at the singular point [1,22,25,26].

The apparent discrepancy between Tai and Rozenfeld [14] and Rahmat-Samii [17] for the electric dyadic Green's function for a rectangular cavity simply does not exist. It will be shown in the next subsection that their expressions are mathematically identical.

E. Nonexistence of Discrepancy in the Electric Dyadic Green's Function for the Rectangular Cavity

Recent research activities in the singularity of the electric dyadic Green's function have been stimulated to a great extent by the apparent discrepancy in the literature regarding the singularity of the electric dyadic Green's function for the rectangular cavity [14,17]. This apparent discrepancy was pointed out by Yaghjian, who developed a new theory in an attempt to resolve it [19-21]. In the following, it will be proved that the expressions of Tai and Rozenfeld [14] and Rahmat-Samii [17] are mathematically identical except for a sign error in the latter. The apparent discrepancy was probably due to a superficial observation. The term involving the Dirac-delta function can be easily taken for the singularity while the overlooked remaining terms may contain singularities concealed in the innocent-looking series of sinusoidal functions. The electric dyadic Green's function derived by Tai and Rozenfeld is of the following form:

$$\underline{\underline{G}}_e^T = -\frac{1}{k^2}\,\hat{z}\,\hat{z}\,\delta(|\underline{r}-\underline{r}'|) + \sum_{m,n} C_{mn}^* \left[(\underline{m}_e\,\underline{m}'_e + \frac{k_g^2}{k^2}\,\underline{n}_o\,\underline{n}')\, f_{mn} + \frac{k_c^4}{k^2}\,\underline{\ell}_o\,\underline{\ell}'_o\, g_{mn} + \frac{k_c^2}{k^2}\,\underline{n}_o\,\underline{\ell}'_o\,\frac{\partial g_{mn}}{\partial z} - \frac{k_c^2}{k^2}\,\underline{\ell}_o\,\underline{n}'_o\,\frac{\partial f_{mn}}{\partial z} \right] \qquad (16)$$

where $e^{-j\omega t}$ is implicit and suppressed, and

$$C_{mn}^* = \frac{2\,(2-\delta_o)}{abk_c^2\,k_g \sin k_g C} \qquad (17)$$

$$f_{mn} = \begin{Bmatrix} \text{Sink}_g(c-z)\,\text{Sink}_g z' \\ \text{Sink}_g z\ \text{Sink}_g(c-z') \end{Bmatrix} \quad \text{for } z \gtrless z' \tag{18}$$

$$g_{mn} = \begin{Bmatrix} \text{Cosk}_g(c-z)\,\text{Cosk}_g z' \\ \text{Cosk}_g z\ \text{Cosk}_g(c-z') \end{Bmatrix} \quad \text{for } z \gtrless z' \tag{19}$$

$$\underline{\ell}_o = \phi_o \hat{z} \tag{21}$$

$$\underline{m}_e = \nabla_t \phi_e \times \hat{z} \tag{22}$$

$$\underline{n}_o = \nabla_t \phi_o \tag{23}$$

$$\phi_o = \text{Sink}_x x\ \text{Sink}_y y \tag{24}$$

$$\phi_e = \text{Cosk}_x x\ \text{Cosk}_y y \tag{25}$$

$$k_x = \frac{m\pi}{a}\ ,\ k_y = \frac{n\pi}{b}\ ,\ k_z = \frac{\ell\pi}{c}\ ,\ \ell, m, n = 0,1,2,\ \ldots \tag{26a}$$

$$k_c = [k^2 - k_x^2 - k_y^2 - k_z^2]^{1/2} \tag{26b}$$

$$k_g = [k^2 - k_c^2]^{1/2} \tag{26c}$$

$$\delta_o = \begin{cases} 1 & \text{if } \ell \text{ or } m \text{ or } n = 0 \\ o & \text{if } \ell, m, n \neq 0 \end{cases} \tag{27}$$

The expression by Rahmat-Samii had an error in sign resulting from misprint or trivial human errors. After correction, his expression reads, in terms of the $e^{j\omega t}$ convention chosen by him,

$$\underline{\underline{G}}_e^R = -\frac{1}{k^2}\,\underline{\underline{I}}\,\delta(|\underline{r}-\underline{r}'|) - \frac{1}{k^2}\sum_{n=0}^{\infty}\sum_{m=0}^{\infty}\sum_{\ell=0}^{\infty} \frac{\varepsilon_{on}\varepsilon_{om}\varepsilon_{o\ell}}{abc\left[k^2-\left(\frac{n\pi}{a}\right)^2-\left(\frac{m\pi}{b}\right)^2-\left(\frac{\ell\pi}{c}\right)^2\right]}$$

$$\left\{\left[\left(\frac{m\pi}{b}\right)^2+\left(\frac{\ell\pi}{c}\right)^2\right]\text{Cos}\ \frac{n\pi x}{a}\ \text{Cos}\ \frac{n\pi x'}{a}\ \text{Sin}\ \frac{m\pi y}{b}\ \text{Sin}\ \frac{m\pi y'}{b}\right.$$

$$\text{Sin}\ \frac{\ell\pi z}{c}\ \text{Sin}\ \frac{\ell\pi z'}{c}\ \hat{x}\,\hat{x} + \left[\left(\frac{\ell\pi}{c}\right)^2 + \left(\frac{n\pi}{a}\right)^2\right]\ \text{Sin}\ \frac{n\pi x}{a}\ \text{Sin}\ \frac{n\pi x'}{a}$$

$$\text{Cos}\ \frac{m\pi y}{b}\ \text{Cos}\ \frac{m\pi y'}{b}\ \text{Sin}\ \frac{\ell\pi z}{c}\ \text{Sin}\ \frac{\ell\pi z'}{c}\ \hat{y}\,\hat{y} + \left[\left(\frac{n\pi}{a}\right)^2 + \left(\frac{m\pi}{b}\right)^2\right]$$

$$\text{Sin}\ \frac{n\pi x}{a}\ \text{Sin}\ \frac{n\pi x'}{a}\ \text{Sin}\ \frac{m\pi y}{b}\ \text{Sin}\ \frac{m\pi y'}{b}\ \text{Cos}\ \frac{\ell\pi z}{c}\ \text{Cos}\ \frac{\ell\pi z'}{c}\hat{z}\,\hat{z}$$

$$-\frac{n\pi}{a}\frac{m\pi}{b}\ \text{Cos}\ \frac{n\pi x}{a}\ \text{Sin}\ \frac{n\pi x'}{a}\ \text{Sin}\ \frac{m\pi y}{b}\ \text{Cos}\ \frac{m\pi y'}{b}\ \text{Sin}\ \frac{\ell\pi z}{c}\ \text{Sin}\ \frac{\ell\pi z'}{c}\ \hat{x}\hat{y}$$

$$-\frac{m\pi}{b}\frac{n\pi}{a}\ \text{Sin}\ \frac{n\pi x}{a}\ \text{Cos}\ \frac{n\pi x'}{a}\ \text{Cos}\ \frac{m\pi y}{b}\ \text{Sin}\ \frac{m\pi y'}{b}\ \text{Sin}\ \frac{\ell\pi z}{c}\ \text{Sin}\ \frac{\ell\pi z'}{c}\ \hat{y}\hat{x}$$

$$-\frac{m\pi}{b}\frac{\ell\pi}{c}\ \text{Sin}\ \frac{n\pi x}{a}\ \text{Sin}\ \frac{n\pi x'}{a}\ \text{Cos}\ \frac{m\pi y}{b}\ \text{Sin}\ \frac{m\pi y'}{b}\ \text{Sin}\ \frac{\ell\pi z}{c}\ \text{Cos}\ \frac{\ell\pi z'}{c}\ \hat{y}\hat{z}$$

$$-\frac{\ell\pi}{c}\frac{m\pi}{b}\ \text{Sin}\ \frac{n\pi x}{a}\ \text{Sin}\ \frac{n\pi x'}{a}\ \text{Sin}\ \frac{m\pi y}{b}\ \text{Cos}\ \frac{m\pi y'}{b}\ \text{Cos}\ \frac{\ell\pi z}{c}\ \text{Sin}\ \frac{\ell\pi z'}{c}\ \hat{z}\hat{y}$$

$$-\frac{\ell\pi}{c}\frac{n\pi}{a}\ \text{Sin}\ \frac{n\pi x}{a}\ \text{Cos}\ \frac{n\pi x'}{a}\ \text{Sin}\ \frac{m\pi y}{b}\ \text{Sin}\ \frac{m\pi y'}{b}\ \text{Cos}\ \frac{\ell\pi z}{c}\ \text{Sin}\ \frac{\ell\pi z'}{c}\ \hat{z}\hat{x}$$

$$-\frac{n\pi}{a}\frac{\ell\pi}{c}\ \text{Cos}\ \frac{n\pi x}{a}\ \text{Sin}\ \frac{n\pi x'}{a}\ \text{Sin}\ \frac{m\pi y}{b}\ \text{Sin}\ \frac{m\pi y'}{b}\ \text{Sin}\ \frac{\ell\pi z}{c}\ \text{Cos}\ \frac{\ell\pi z'}{c}\ \hat{x}\hat{z}\Bigg\} \qquad (28)$$

where $\varepsilon_{om} = \begin{cases} 1 & \text{if } m = 0 \\ 2 & \text{otherwise.} \end{cases}$ (29)

Note that m and n are exchanged between the notations of Equations (16) and Equation (28). The discrepancy, according to Yaghjian [20], was that the term involving the Dirac-delta function was $-\frac{1}{k^2}\hat{z}\,\hat{z}$ in Equation (16) of Tai and Rozenfeld, but was $-\frac{1}{k^2}\underline{\underline{I}}$ in Rahmat-Samii's expression of Equation (28), as shown in Table 1. We will show that Equation (16) is identical to Equation (28) and therefore no discrepancy exists. We begin with Equation (24) of Tai and Rozenfeld [14] as follows:

$$\underline{G}_e^T = \sum_{\ell,m,n} \frac{C_{mn}}{K^2 - k^2}\left[\underline{m}_e\underline{m}'_e\ \text{Sin}\ k_z z\ \text{Sin}\ k_z z'\right.$$

$$\left. + \frac{k_g^2}{k^2}\underline{n}_o\underline{n}'_o\ \text{Sin}\ k_z z\ \text{Sin}\ k_z z'\right.$$

$$+ \frac{k_c^2(k^2 - k_z^2)}{k^2} \underline{\ell}_o \underline{\ell}_o' \text{ Cos } k_z z \text{ Cos } k_z z'$$

$$- \frac{k_z k_c^2}{k^2} (\underline{\ell}_o \underline{n}_o' \text{ Cos } k_z z \text{ Sin } k_z z'$$

$$+ \underline{n}_o \underline{\ell}_o' \text{ Sin } k_z z \text{ Cos } k_z z')] \, , \qquad (30)$$

where

$$K^2 = k_x^2 + k_y^2 + k_z^2 \qquad (31)$$

Substitution of Equations (17-27) into Equation (30) yields

$$\underline{G}_e^T = - \frac{1}{k^2} \sum_{n=0}^{\infty} \sum_{m=0}^{\infty} \sum_{\ell=0}^{\infty} \frac{4(2-\delta_o)}{abc[k^2 - K^2]}$$

$$\Big\{ \hat{x}\hat{x}(k^2 - k_x^2) \text{ Cosk}_x x \text{ Cosk}_x x' \text{ Sink}_y y \text{ Sink}_y y' \text{ Sink}_z z \text{ Sink}_z z'$$

$$+ \hat{y}\hat{y}(k^2 - k_y^2) \text{ Sink}_x x \text{ Sink}_x x' \text{ Cosk}_y y \text{ Cosk}_y y' \text{ Sink}_z z \text{ Sink}_z z'$$

$$+ \hat{z}\hat{z}(k^2 - k_z^2) \text{ Sink}_x x \text{ Sink}_x x' \text{ Sink}_y y \text{ Sink}_y y' \text{ Cosk}_z z \text{ Cosk}_z z'$$

$$+ \hat{x}\hat{y}(- k_x k_y) \text{ Cosk}_x x \text{ Sink}_x x' \text{ Sink}_y y \text{ Cosk}_y y' \text{ Sink}_z z \text{ Sink}_z z'$$

$$+ \hat{y}\hat{x}(- k_x k_y) \text{ Sink}_x x \text{ Cosk}_x x' \text{ Cosk}_y y \text{ Sink}_y y' \text{ Sink}_z z \text{ Sink}_z z'$$

$$+ \hat{y}\hat{z}(- k_z k_y) \text{ Sink}_x x \text{ Sink}_x x' \text{ Cosk}_y y \text{ Sink}_y y' \text{ Sink}_z z \text{ Cosk}_z z'$$

$$+ \hat{z}\hat{y}(- k_z k_y) \text{ Sink}_x x \text{ Sink}_x x' \text{ Sink}_y y \text{ Cosk}_y y' \text{ Cosk}_z z \text{ Sink}_z z'$$

$$+ \hat{x}\hat{z}(- k_z k_x) \text{ Cosk}_x x \text{ Sink}_x x' \text{ Sink}_y y \text{ Sink y}' \text{ Sink}_z z \text{ Cosk}_z z'$$

$$+ \hat{z}\hat{x}(- k_z k_x) \text{ Sink}_x x \text{ Cosk}_x x' \text{ Sink}_y y \text{ Sink}_y y' \text{ Cosk}_z z \text{ Sink}_z z' \Big\} \, , \qquad (32)$$

Now

$$-\frac{1}{k^2}\sum_{n=0}^{\infty}\sum_{m=0}^{\infty}\sum_{\ell=0}^{\infty}\frac{4(2-\delta_o)}{abc[k^2-K^2]}(k^2-k_x^2)\,\mathrm{Cosk}_x x\,\mathrm{Cosk}_x x'\,\mathrm{Sink}_y y\,\mathrm{Sink}_y y'$$

$$\mathrm{Sink}_z z\,\mathrm{Sink}_z z'$$

$$= -\frac{1}{k^2}\delta(|\underline{r}-\underline{r}'|) - \frac{1}{k^2}\sum_{n=0}^{\infty}\sum_{m=0}^{\infty}\sum_{\ell=0}^{\infty}\frac{4(2-\delta_o)}{abc}\,\frac{k_y^2+k_z^2}{k^2-K^2}$$

$$\mathrm{Cosk}_x x\,\mathrm{Cosk}_x x'\,\mathrm{Sink}_y y\,\mathrm{Sink}_y y'\,\mathrm{Sink}_z z\,\mathrm{Sink}_z z' \quad , \qquad (33)$$

$$-\frac{1}{k^2}\sum_{n=0}^{\infty}\sum_{m=0}^{\infty}\sum_{\ell=0}^{\infty}\frac{4(2-\delta_o)}{abc[k^2-K^2]}(k^2-k_y^2)\,\mathrm{Sink}_x x\,\mathrm{Sink}_x x'$$

$$\mathrm{Cosk}_y y\,\mathrm{Cosk}_y y'\,\mathrm{Sink}_z z\,\mathrm{Sink}_z z'$$

$$= -\frac{1}{k^2}\delta(|\underline{r}-\underline{r}'|) - \frac{1}{k^2}\sum_{n=0}^{\infty}\sum_{m=0}^{\infty}\sum_{\ell=0}^{\infty}\frac{4(2-\delta_o)}{abc}\,\frac{k_x^2+k_z^2}{k^2-K^2}$$

$$\mathrm{Sink}_x x\,\mathrm{Sink}_x x'\,\mathrm{Cosk}_y y\,\mathrm{Cosk}_y y'\,\mathrm{Sink}_z z\,\mathrm{Sink}_z z' \quad , \qquad (34)$$

and

$$-\frac{1}{k^2}\sum_{n=0}^{\infty}\sum_{m=0}^{\infty}\sum_{\ell=0}^{\infty}\frac{4(2-\delta_o)}{abc[k^2-K^2]}(k^2-k_z^2)\,\mathrm{Sink}_x x\,\mathrm{Sink}_x x'\,\mathrm{Sink}_y y\,\mathrm{Sink}_y y'$$

$$\mathrm{Cosk}_z z\,\mathrm{Cosk}_z z' = -\frac{1}{k^2}\delta(|\underline{r}-\underline{r}'|) - \frac{1}{k^2}\sum_{n=0}^{\infty}\sum_{m=0}^{\infty}\sum_{\ell=0}^{\infty}\frac{4(2-\delta_o)}{abc}$$

$$\frac{k_x^2+k_y^2}{k^2-K^2}\,\mathrm{Sink}_x x\,\mathrm{Sink}_x x'\,\mathrm{Sink}_y y\,\mathrm{Sink}_y y'\,\mathrm{Cosk}_z z\,\mathrm{Cosk}_z z' \qquad (35)$$

Substitution of Equations (33-35) into Equation (32) yields an expression of $\underline{G}_e^T$ identical to $\underline{G}_e^R$ of Equation (28), with the understanding that m and n are exchanged and that

$$4(2-\delta_o) = \varepsilon_{on}\varepsilon_{om}\varepsilon_{o\ell} \tag{36}$$

if at least two of the three integers, m, n and ℓ, are nonzeros (when two or more of them are zero, the series term is zero). We can also prove directly that Equations (16) and (28) are identical either by substituting only Equation (35) into Equation (32) or by using Equations (33), (34) and the following relations

$$\sum_{\ell=0}^{\infty} \frac{1}{K^2-k^2}\ \mathrm{Sink}_z z\ \mathrm{Sink}_z z' = \frac{c}{2k_g \mathrm{Sink}_g c} \begin{Bmatrix} \mathrm{Sink}_g(c-z)\mathrm{Sink}_g z' \\ \mathrm{Sink}_g z\ \mathrm{Sink}_g(c-z') \end{Bmatrix} \quad z_<^>z' \tag{37}$$

$$\sum_{\ell=0}^{\infty} \frac{\varepsilon_{o\ell}}{K^2-k^2}\ \mathrm{Cosk}_z z\ \mathrm{Cosk}_z z' = \frac{-c}{k_g \mathrm{Sink}_g c} \begin{Bmatrix} \mathrm{Cosk}_g(c-z)\mathrm{Cosk}_g z' \\ \mathrm{Cosk}_g z\ \mathrm{Cosk}_g(c-z') \end{Bmatrix} \quad z_<^>z' \tag{38}$$

$$\sum_{\ell=0}^{\infty} \frac{k_z}{K^2-k^2}\ \mathrm{Sink}_z z\ \mathrm{Cosk}_z z' = \frac{-c}{2\mathrm{Sink}_g c} \begin{Bmatrix} \mathrm{Sin}(c-z)\mathrm{Cosk}_g z' \\ -\mathrm{Sink}_g z\ \mathrm{Cosk}_g(c-z') \end{Bmatrix} \quad z_<^>z' \tag{39}$$

and

$$\sum_{\ell=0}^{\infty} \frac{k_z}{K^2-k^2}\ \mathrm{Cosk}_z z\mathrm{Sink}_z z' = \frac{c}{2\mathrm{Sink}_g c} \begin{Bmatrix} -\mathrm{Cosk}_g(c-z)\mathrm{Sink}_g z \\ \mathrm{Cosk}_g z\mathrm{Sin}(c-z') \end{Bmatrix} \quad z_<^>z' \tag{40}$$

which were originally employed by Tai and Rozenfeld [14] and are derived in the Appendix of this report. This concludes our proof that there is no contradiction or discrepancy in the electric dyadic Green's function in and outside the source region.

SECTION III

COMPACT RANGE SCATTERING MEASUREMENT

A. Compact Range Scattering Measurement Techniques at 1 GHz.

There has been an increasing amount of interest in the compact range for antenna and scattering measurements. The compact range technique was first implemented in X and Ku bands [29], and was recently extended to 30 GHz [30]. At frequencies below 2 GHz, a number of technical difficulties have long been generally recognized. Major obstacles include the edge diffraction of the reflector, multipath of the illuminating wave, and precision of the instrumentation. These difficulties have been overcome and compact range RCS measurements were extended to as low as 1 GHz.

The cancellation method [31] was employed in the scattering measurement. Figure 4 shows a block diagram illuminating the principle of the set up and Figure 5 shows the physical arrangement of the cancellation network. The use of high-precision microwave components and heavy 1/4 inch semi-rigid cable is essential to obtain a deep null insensitive to temperature variations and vibration. Even the 1/4 inch semi-rigid cable was sometimes found to be sensitive to vibration and had to be fastened to the mounting structure with a damping mechanism. The network was mounted on a plexiglass board which was seated on a layer of foam as shown in Figure 5. Other shock-mounting devices were also placed below the tables, the receivers, the transmitter, the frequency "lock-box", etc. A 1-4 GHz solid-state cavity-tuned source with an output power of 20 to 200 mw was built for the measurement system. When connected with a lock-box, a frequency stability of 1 part in 10^6 was maintained. The dual-channel phase and amplitude receiving system is shown in Figure 6.

The compact range used in this study consists of a 12-foot high by 17-foot wide reflector as shown in Figure 7. The reflector was fed by a 24 in. x 32 1/2 in. rectangular horn, shown in Figure 8, located at a focal distance of about 12 feet. Both the reflector and horns are fabricated by standard methods with average mechanical tolerances. Figure 9 shows a a styrofoam support for the target under test.

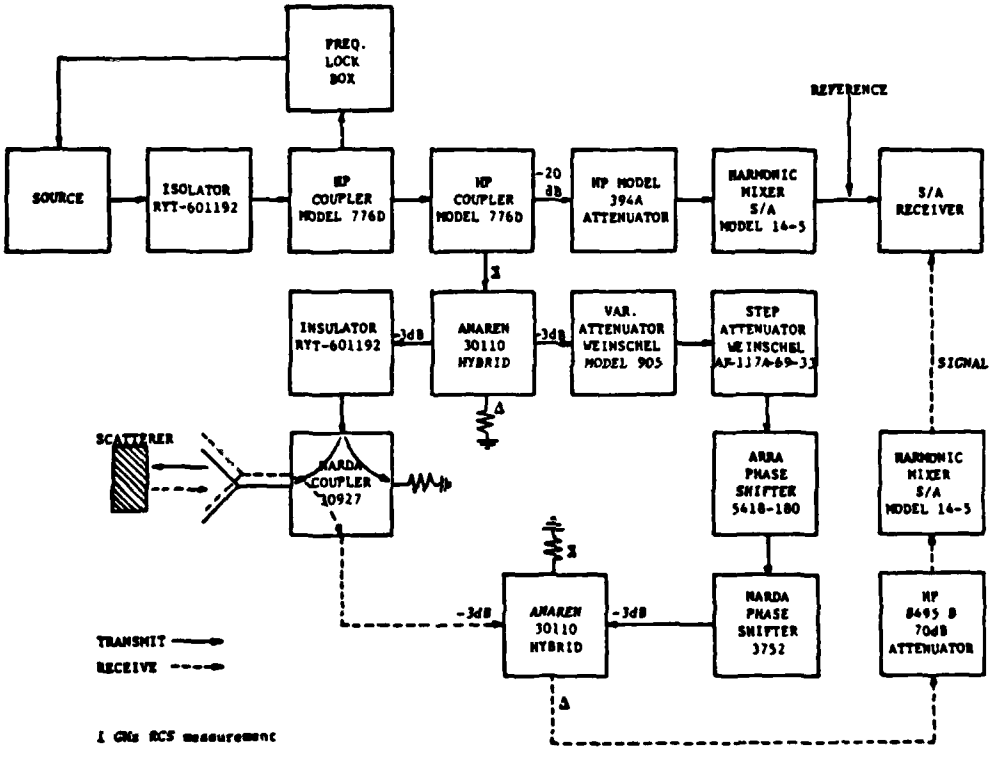

Figure 4. Block diagram for 1 GHz compact range RCS measurement.

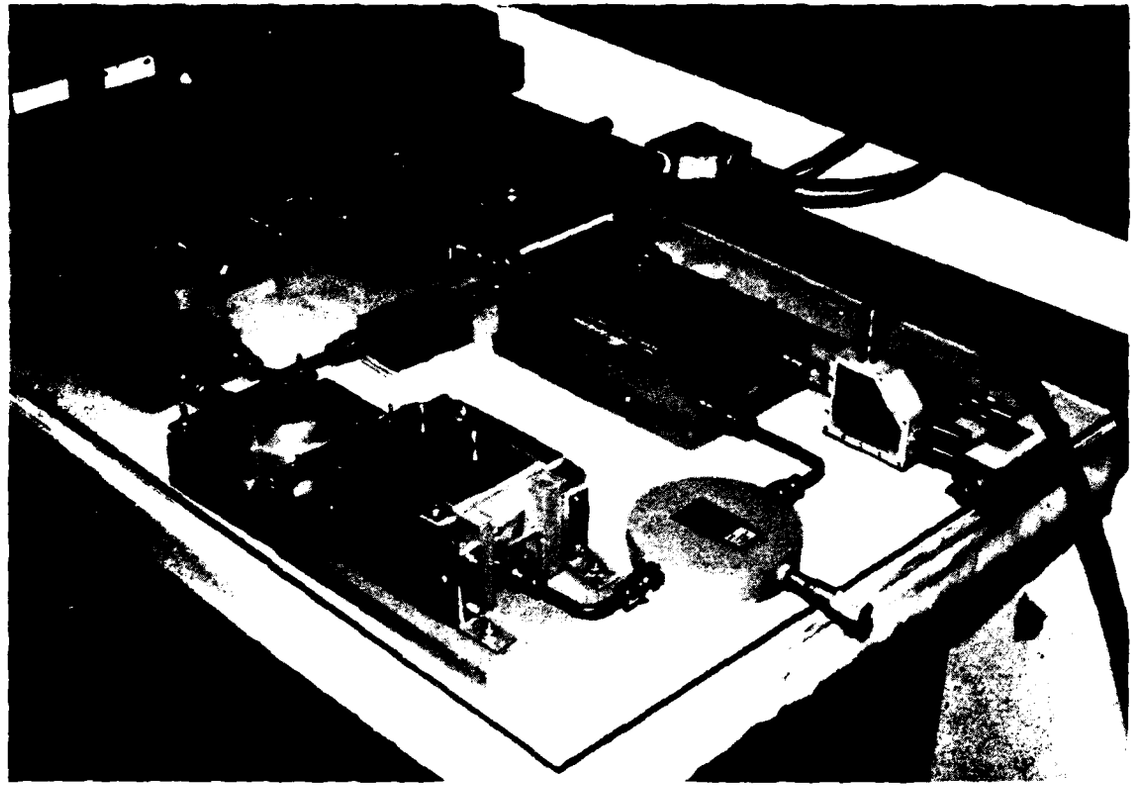

Figure 5. The arrangement of the shock-mounted cancellation network used in the 1 GHz scattering measurements.

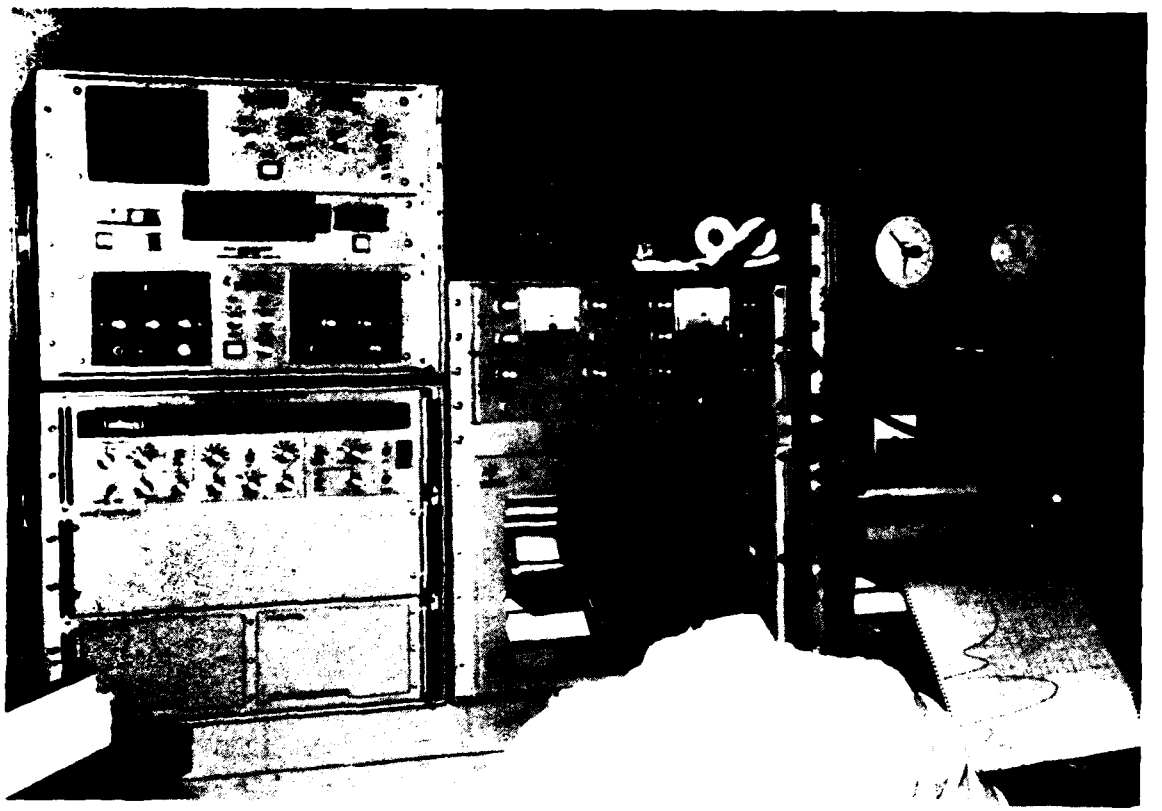

Figure 6. The dual-channel receiving system used in the compact range measurement.

Figure 7. Partial view of the 12-foot high, 16-foot wide reflector used in the compact range.

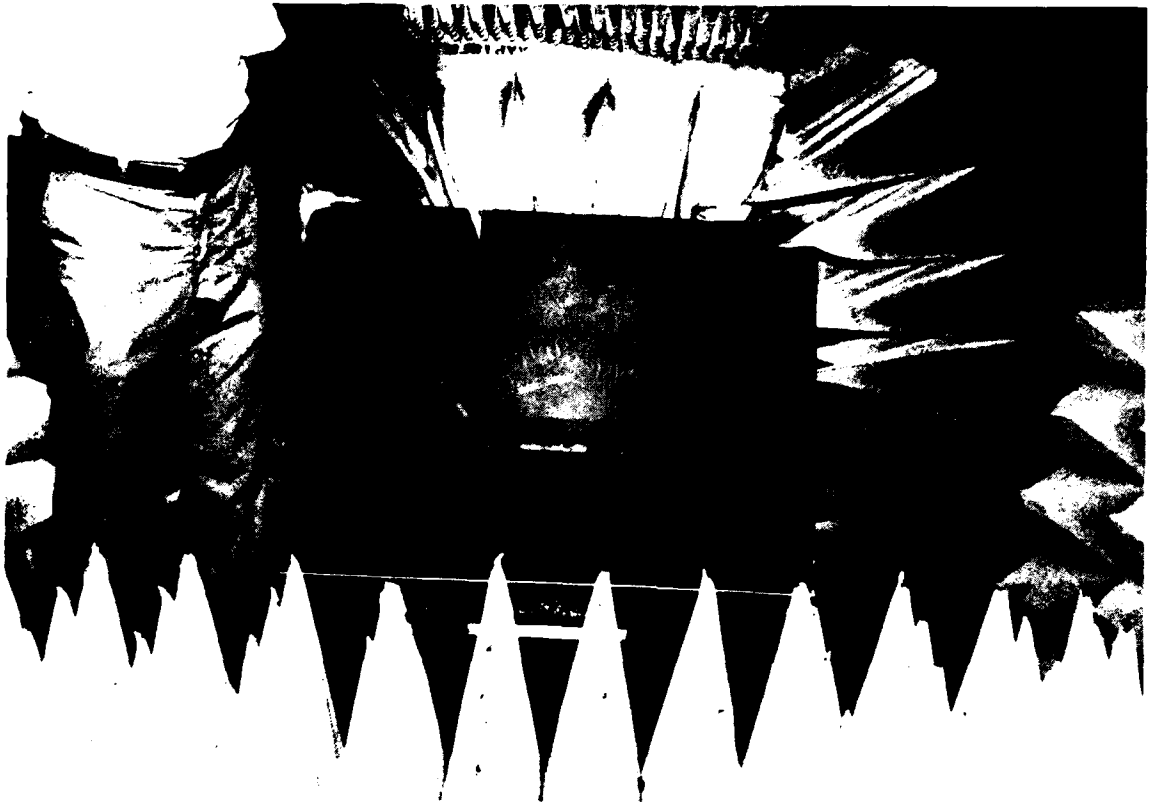

Figure 8. The rectangular horn with a 24 in. x 32 1/2 in. aperture used as a feed for the reflector in the compact range.

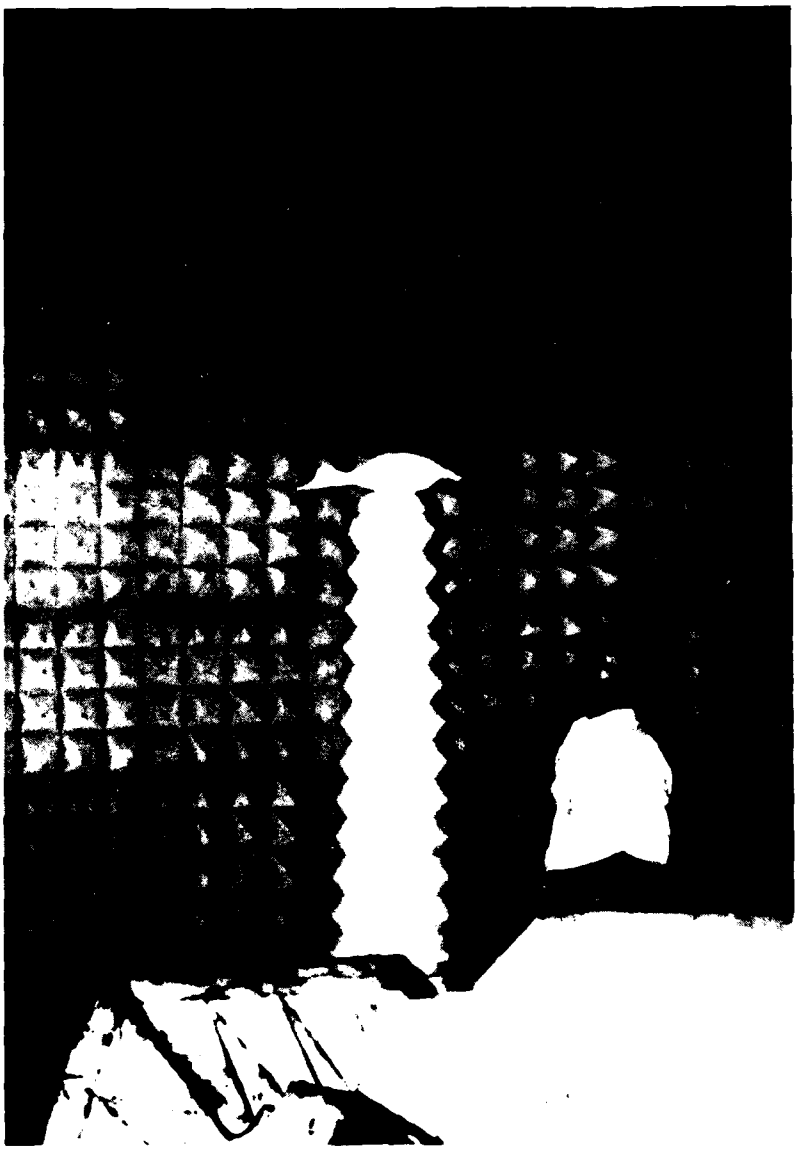

Figure 9. Styrofoam support for the scattering target used in the compact range.

At 1 GHz and lower, the multipath propagation, leakage and parasitic excitation along the source, cable and the components and equipments can cause severe difficulty. In fact, leakage from the source was initially found to be only 30 dB below the illuminating field in the quiet zone. These problems were overcome through careful shielding and the use of microwave absorbers.

The field in the quiet zone was probed with a dipole, and amplitude variations of less than $\pm$1 dB and phase variations less than $\pm$5 degrees over an area of 5 ft. x 3 ft. were achieved. Since the horn used is an ordinary rectangular horn, further improvement in the quiet zone illumination may be achievable by using low-side-lobe feeds such as a corrugated horn.

The ultimate criterion for the radar cross-section range using the cancellation method is the stability and depth of the null achievable. The deeper the null, the smaller echo return the system can detect. Also a stable null insures accurate and consistent measurements. To achieve stability and depth for the null, sufficiently high power and frequency stability of the source are essential. The sensitivity of the receiver is usually sufficient since the environmental noise in the range is usually quite high. In the 1 GHz measurements, we were able to obtain a null depth of -50 dBSM during the day and -60 dBSM in the night, which could be maintained for an average duration of 1.5 to 2 minutes.

The sensitivity of the compact range is displayed by measurements shown in Table 2 on small conducting spheres shown in Figure 10, whose echo areas are accurately known. The close agreement shows that accurate measurements can be made for small scatterers with low echo return. Figure 11a and 11b show measurements on a circular cylinder 2.76 wavelengths long for E and H plane aspect angle. Figure 12a and 12 b show the measured data for flat conducting plates. Figures 13a and 13b show the measured data for rectangular conducting boxes. All these measurements are in good agreement with data in the literature, as can be seen in Figures 10 through 13. However, there is some confusion in the literature concerning the polarization of the data which remains to be clarified.

TABLE II

COMPARISON BETWEEN COMPACT RANGE MEASUREMENT
AND EXACT CALCULATIONS FOR CONDUCTING SPHERES
CALIBRATED WITH THE 0.04403λ SPHERE

Radius in Wavelengths	RCS in dBSM	
	Theoretical	Measured
.04403	-46.14	-46.1
.05503	-40.41	-40.4
.06054	-37.63	-37.6
.06604	-35.45	-35.5
.07154	-33.42	-33.4
.07705	-31.80	-31.8
.10456	-25.44	-25.4
.11010	-22.82	-22.8

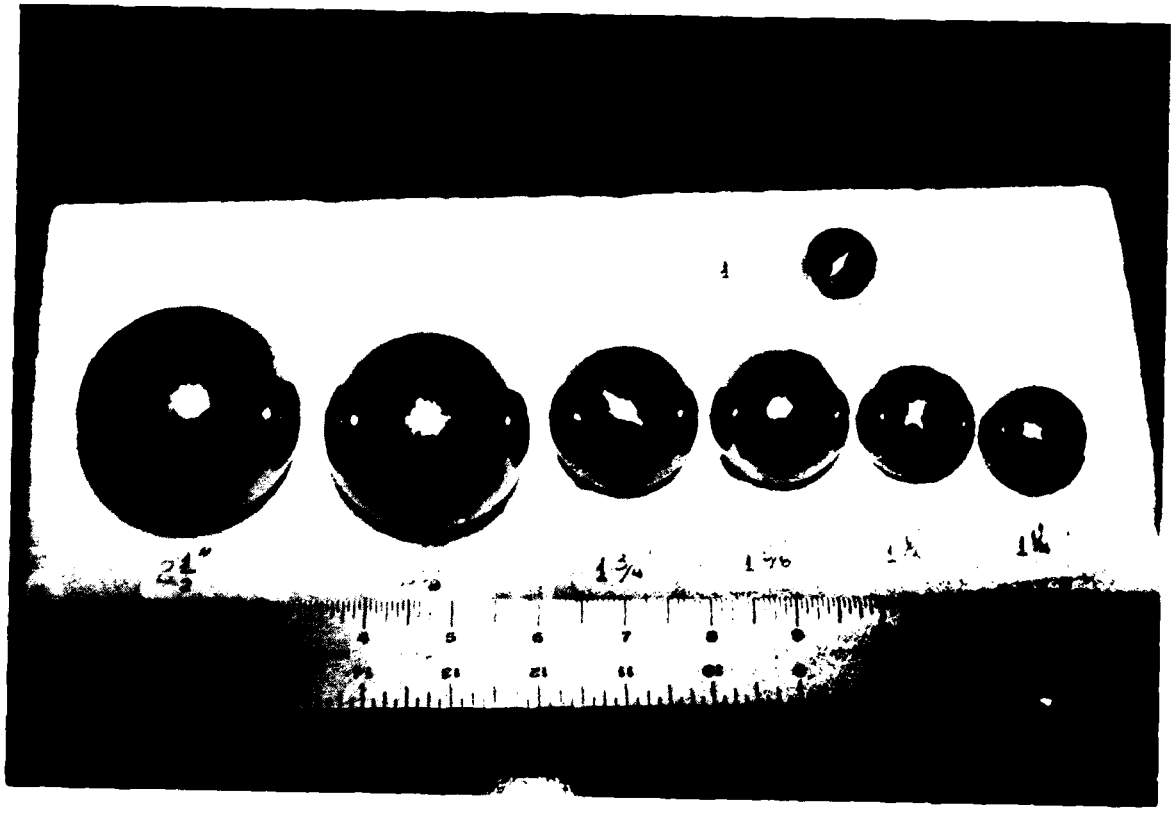

Figure 10. Stainless-steel spheres used in the calibration of the scattering measurement.

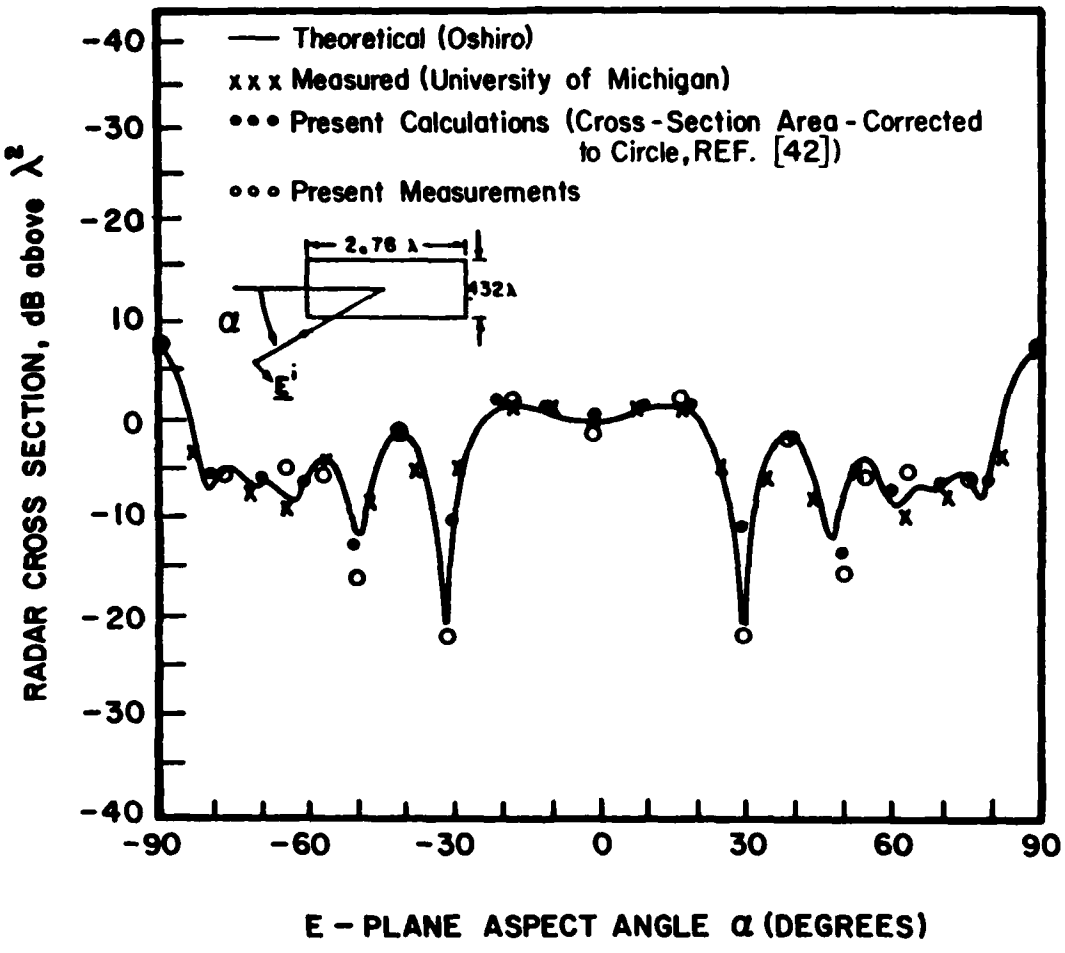

a) E-plane pattern

Figure 11 . Comparison between compact range measurements and other known data for a finite circular cylinder (continued).

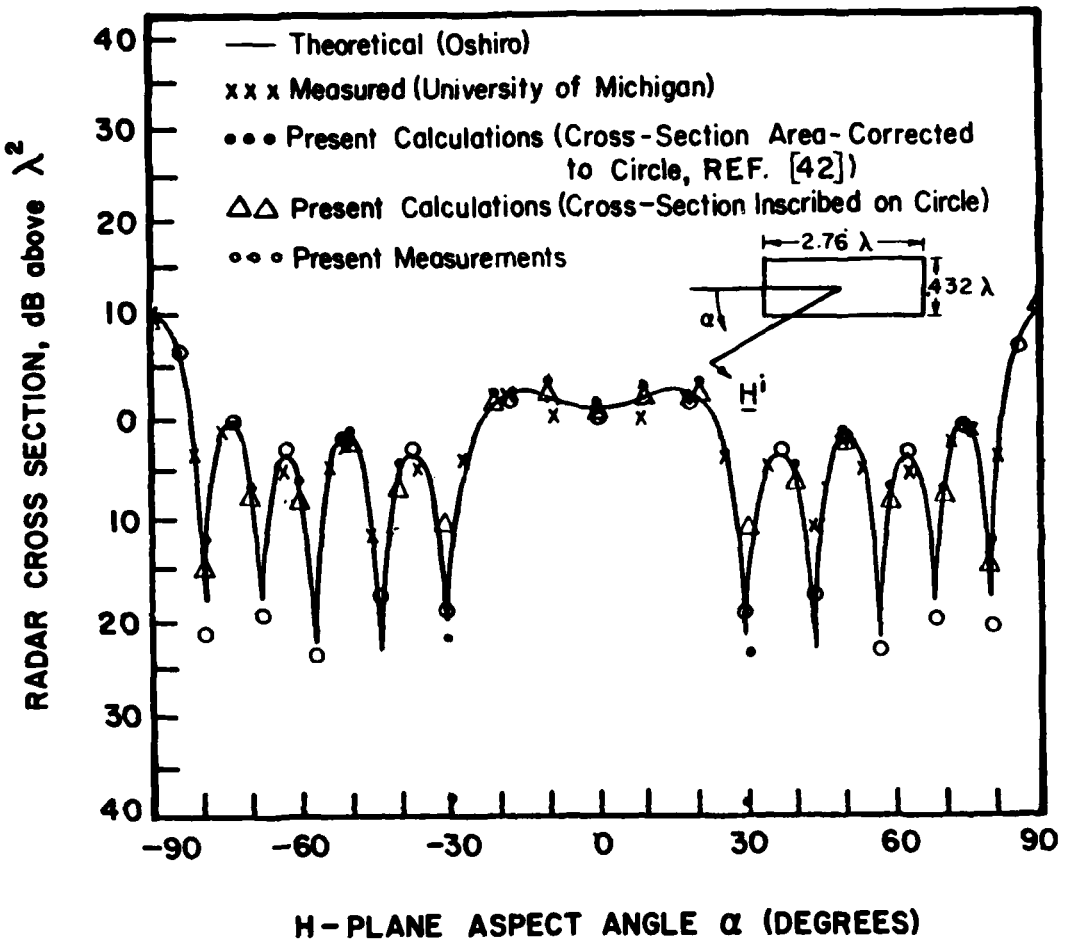

b) H-plane pattern

Figure 11. Comparison between compact range measurements and other known data for a finite circular cylinder.

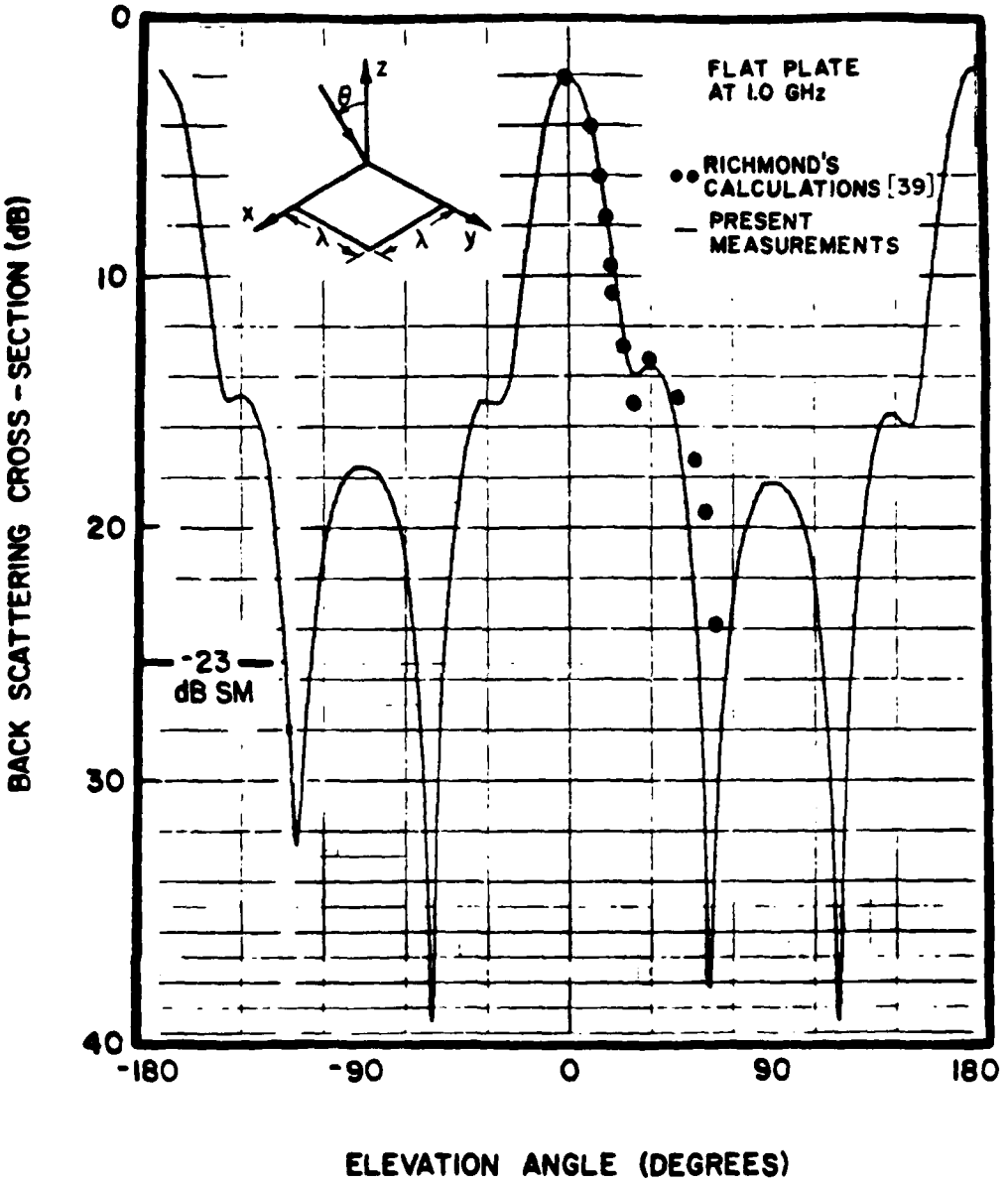

a) Pattern as a function of elevation angle

Figure 12. Comparison of measured backscattering cross-section of a square plate versus incident angle θ, with other known data (continued).

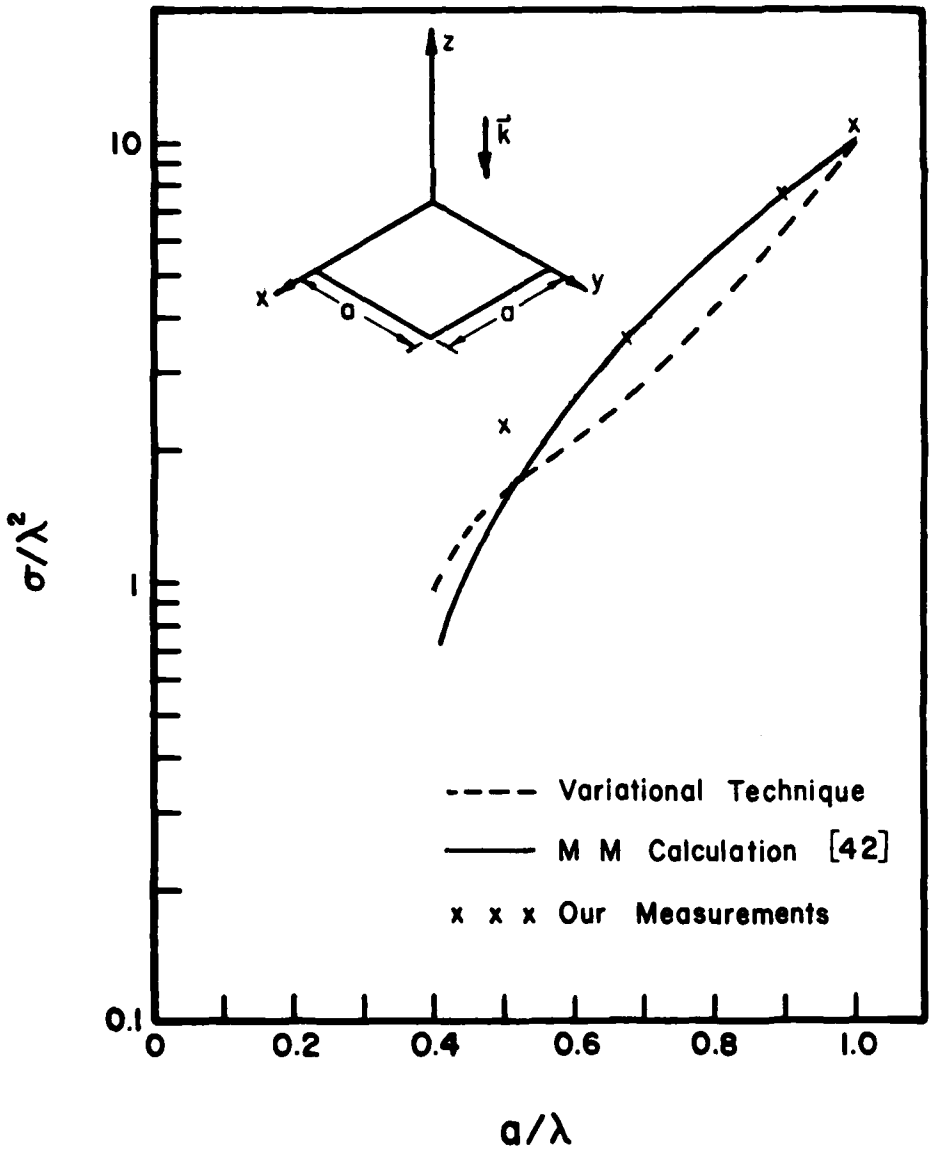

b) Backscatter cross-section as a function of a plate size

Figure 12. Compact range scattering measurement of a flat square conducting plates for normally incident plane wave.

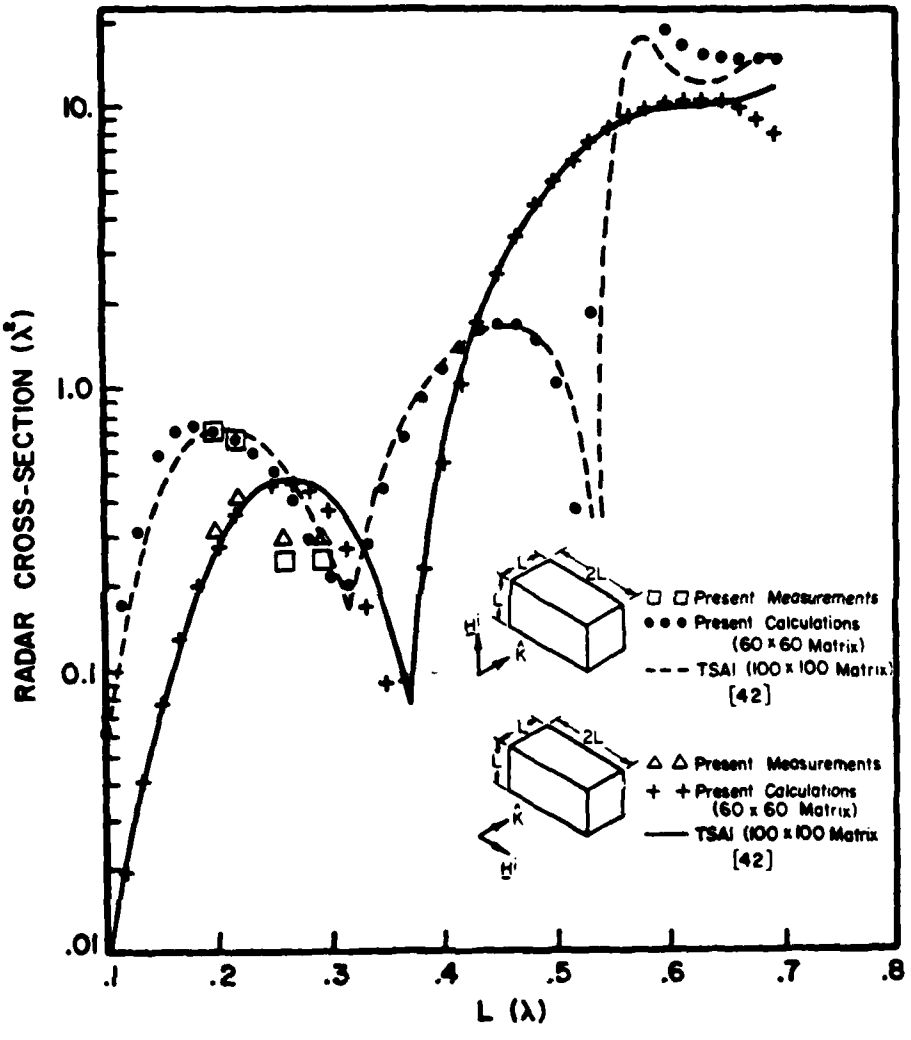

a) Backscatter as a function of length as viewed from the side

Figure 13. Compact range scattering measurement of conducting boxes (continued).

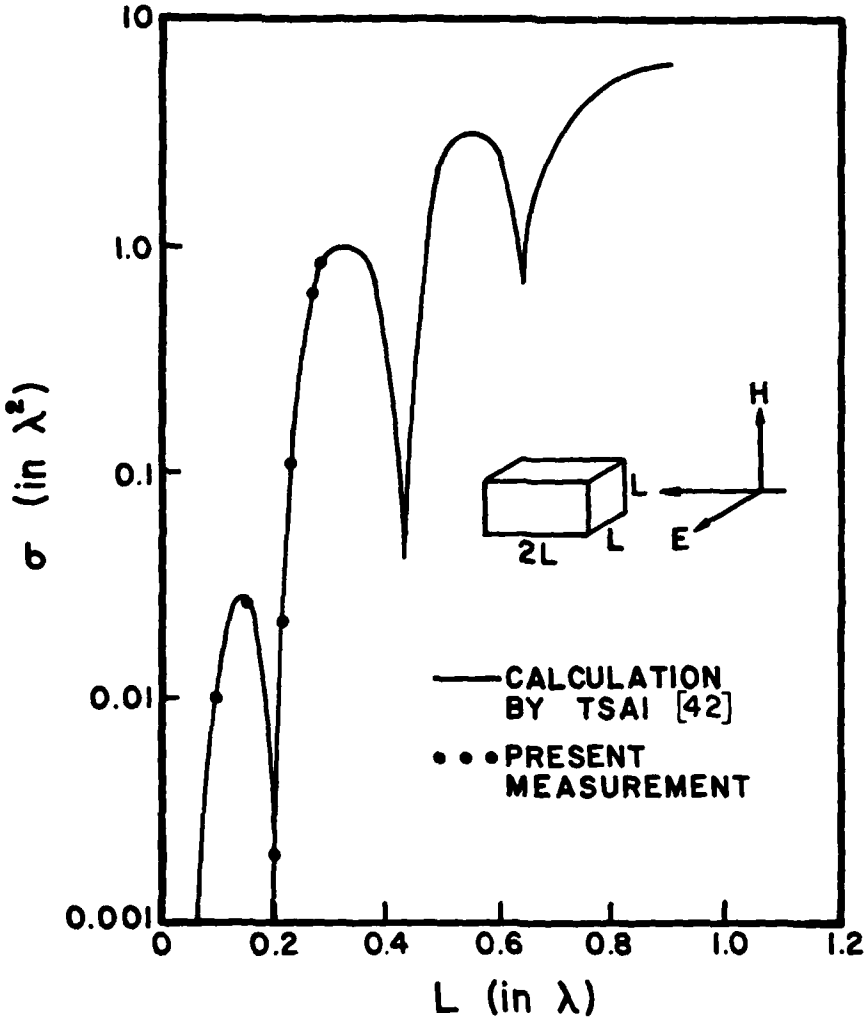

b) Backscatter as a function of length as viewed from the end

Figure 13. Compact range scattering measurement of conducting boxes.

B. Simulation of Biological Bodies

A major difficulty in measurements involving a biological body is the lack of consistency and stability. A living bird or animal undergoes physiological changes all the time. They may feed less today, and they may move during the tests. This difficulty can be very frustrating and the interested reader may consult reference 32 for methods considered by Blacksmith and Mack [33].

Since the physical configuration and the dielectric property are the only parameters involved in the scattering measurements, it is feasible to perform the test on a simulated model. While the simulation model removes the inconsistency and instability inherent in real biological bodies, there exists some degree of uncertainty as to how close the simulation can be realistically accomplished. For example, it is difficult to simulate the feathers, skin, blood vessels, etc. However, feathers and skin have low dielectric constants and can sometimes be conveniently ignored. The blood vessels have high water content but are usually surrounded by muscle tissues which also contain water.

Simulation techniques for biological bodies were developed by Guy [34], who employed various chemicals to simulate the complex dielectric constant of fat, bone, and muscle tissue. His method was used in the fabrication of bird models in this research program.

Before making the model, a styrofoam mold is constructed to hold and support the moist jellied "Super-stuff" plastic. Tho mold is derived from a bird model made of plaster of paris. Figure 14 shows the side and front views of a sitting bird model made of plaster of paris. Figure 15 shows the side and front views of a flying bird model made of plaster of paris. Figure 16 shows the side view of a "Super-stuff" simulated flying Green Wingtail, SB4, in a styrofoam holder.

The "Super-stuff" simulated muscle tissue is composed of the following materials

Saline solution (12g salt/liter)	76.5% (by weight)
Powdered polyethylene	15.2%
Super-stuff	8.4% .

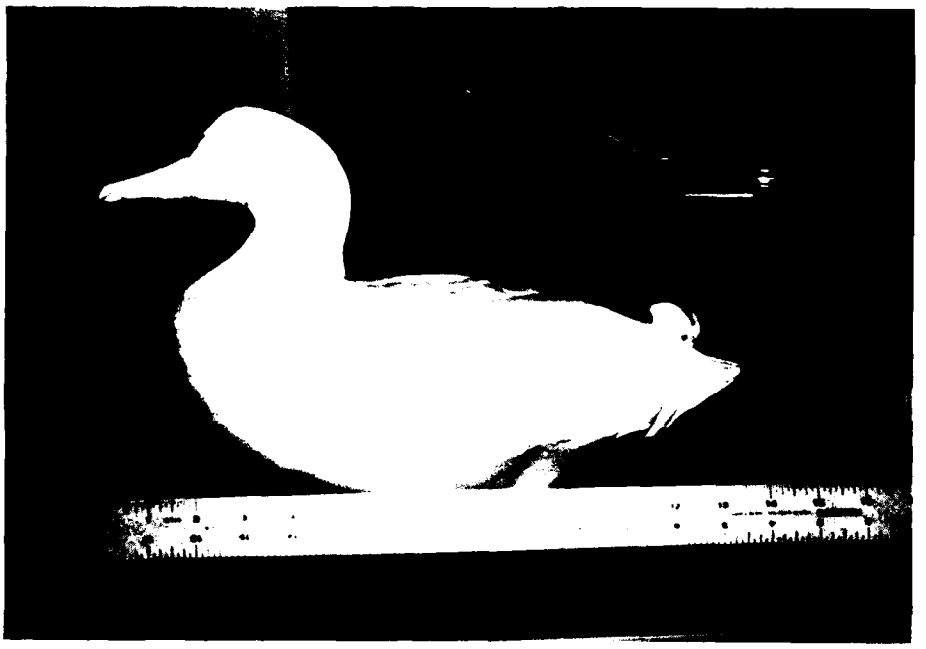

(a) Side view

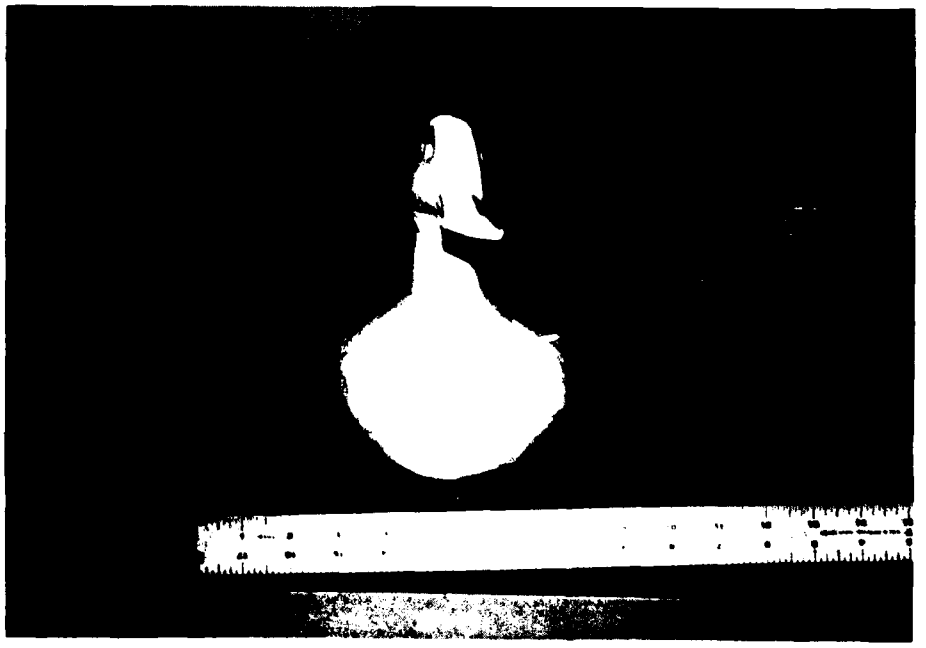

(b) Front view

Figure 14. Side and front views of a sitting bird made of plaster of paris.

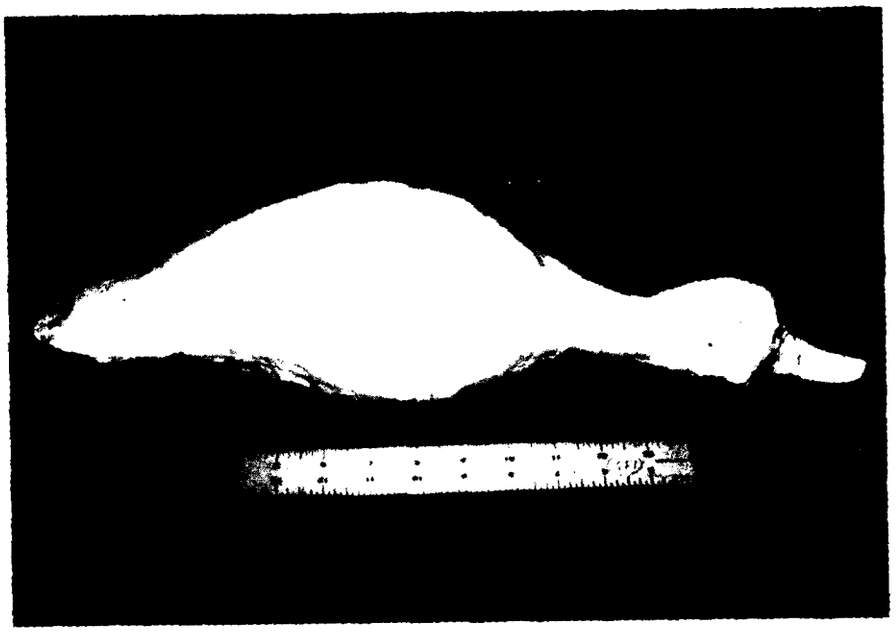

(a) Side view

(b) Front view

Figure 15. Side and front views of a flying bird made of plaster of paris.

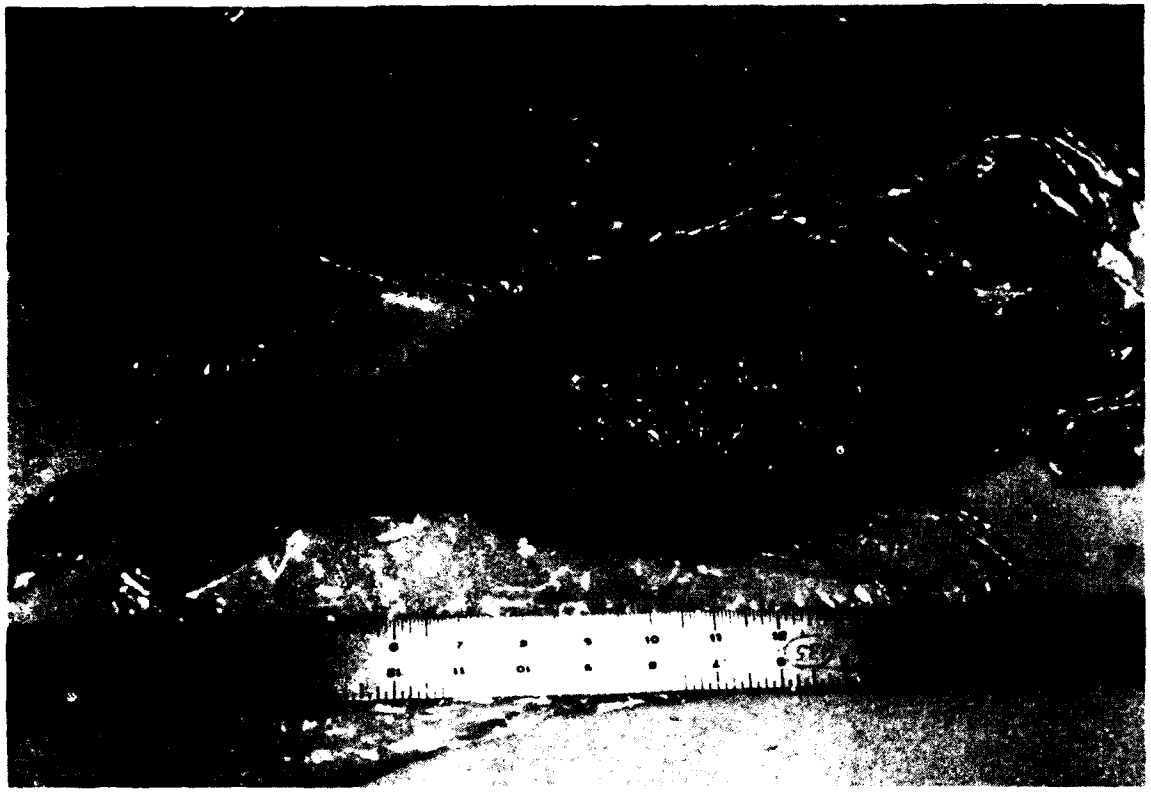

Figure 16. Side view of a "Super-stuff" simulated bird, SB4, in a styrofoam holder.

The "Super-stuff" is a jelling agent manufactured by Oil Center Research Corp. in Laffayette, Louisiana. The mixing process, which was improved here by trial and error, is critical to the homogeneity of the simulated tissue. Spectroscopic-grade salt is first added to deionized water in a blending mixer in an oven. After reaching 200°F the solution is stirred for about 2 minutes. Fine polyethylene powder is then slowly poured into the solution which is now being stirred at high speed. After half of the polyethelene powder is poured in, the rest of the powder is mixed with the super-stuff and poured into the solution being stirred at high speed. The temperature and stirring help to remove bubbles and attain homogeneity. The temperature is then raised to 450°F for two minutes and the mixture is then allowed to cool.

Although it is usually possible to make a simulation model to meet the required dimensions, it is not easy to obtain the required complex dielectric constant with high accuracy. In order to insure reasonable accuracy in the model, the in-vivo probe measurement technique [35] was used to determine the complex permittivity of the model. Ordinarilly there is about 5 percent error in this dielectric constant measurement. In all the simulation models measured, the disagreements between the anticipated and measured complex permittivity were mostly within 5 percent of each other.

SECTION IV

NUMERICAL COMPUTATIONS FOR VARIOUS DIELECTRIC SCATTERERS

An exact solution for three-dimensional dielectric scatterers in free space exists only for the sphere. For scatterers of arbitrary shapes, numerical analyses employing the volume integral equation have been conducted [25,26,36,37]. There are other numerical and approximate methods which are devoted to the estimates of SAR (Specific Absorption Rate) [38], which is the average power absorbed per unit weight of the biological body. However, there appears to be little research in the analysis of the scattering cross section of arbitrarily-shaped dielectric and biological bodies.

In this section we discuss the use of the volume integral equation to compute the scattering cross section of three-dimensional arbitrarily-shaped dielectric bodies including rectangular and I-shaped boxes, spheres, finite circular cylinders, and simulated birds.

The basic volume integral equation has been discussed in detail in Reference 26. The dielectric body can be replaced by an equivalent volume current $\underline{J}$ such that

$$\underline{J} = j\omega\,(\varepsilon - \varepsilon_o)\,\underline{E} \tag{41}$$

where ω is the angular frequency, $\underline{E}$ is the electric field, ε_o and ε are the complex permittivity in free space and the dielectric body, respectively. The volume integral equation in terms of the unknown $\underline{J}$ is

$$\int_V \underline{G}(\underline{r},\underline{r}')\,\underline{J}\,(\underline{r}')\,dv - \frac{\varepsilon + 2\varepsilon_o}{3j\omega\varepsilon_o[\varepsilon-\varepsilon_o]}\,\underline{J}\,(\underline{r}) = \underline{E}^i(\underline{r}), \tag{42}$$

where

$$\underline{G}\,(\underline{r},\underline{r}') = -j\omega\mu\left(\underline{I} + \frac{\nabla\nabla}{k}\right)\frac{\exp\,(-jk|\underline{r}-\underline{r}'|)}{4\pi|\underline{r}-\underline{r}'|}\,,$$

$\underline{E}^i\,(\underline{r})$ = incident electric field intensity,

$\int_v$ = Principal volume integral excluding the singular point at $|\underline{r}-\underline{r}'|$

$\underline{I}$ = unit dyad

The solution of Equation (42) can be carried out by the method of moments. The dielectric body, generally heterogeneous, is divided into rectangular box cells and the equivalent current is expanded into a series of pulse functions, each of which is uniform in one cell and vanishes outside the cell. The Dirac-delta function, defined at the center of each volume cell, is used as the weighting function. By taking a scalar product on both sides of equation (42) with a weighting function and integrating over V, we generate a system of linear equations which is then solved numerically on a computer. The scattering cross section is then computed in terms of the equivalent current $\underline{J}$ by numerical integration.

Numerical computations have been conducted for dielectric and biological bodies of various shapes including cubes, cylinders, spheres, rectangular and I-shaped boxes, and simulated birds. Good agreements have been observed for the field distribution inside the dielectric body in comparison with the data from Michigan State University [26,36,37]. For scattering calculations, the only data available in the literature were for spheres and finite circular cylinders. The present calculation showed correctly the sharp resonance behavior of the back-scatter cross section as a function of frequency. But the frequencies of resonance were about 20 percent lower than those based on the Mie series computation. This discrepancy could be due to the reduced apparent size of the sphere in the simulation using rectangular cells. Agreement with the finite cylinder is good. These results are presented in detail as follows.

A. Scatterers of Simple Shapes

Figure 17 shows the calculated back-scatter cross section for a finite dielectric cylinder in comparison with the data from Richmond [39]. Figure 18 shows the geometry of a rectangular box of saline water and the way the volume cells are divided and numbered. The calculated field distribution is displayed in Tables 3a, 3b and 3c for the x-component, z-component and total field of the electric field intensity. They are in good agreement with Michigan State data [36]. Figure 19 shows the calculated back-scatter cross section of this rectangular box of saline water in comparison with the measured data obtained at the Georgia Tech compact range.

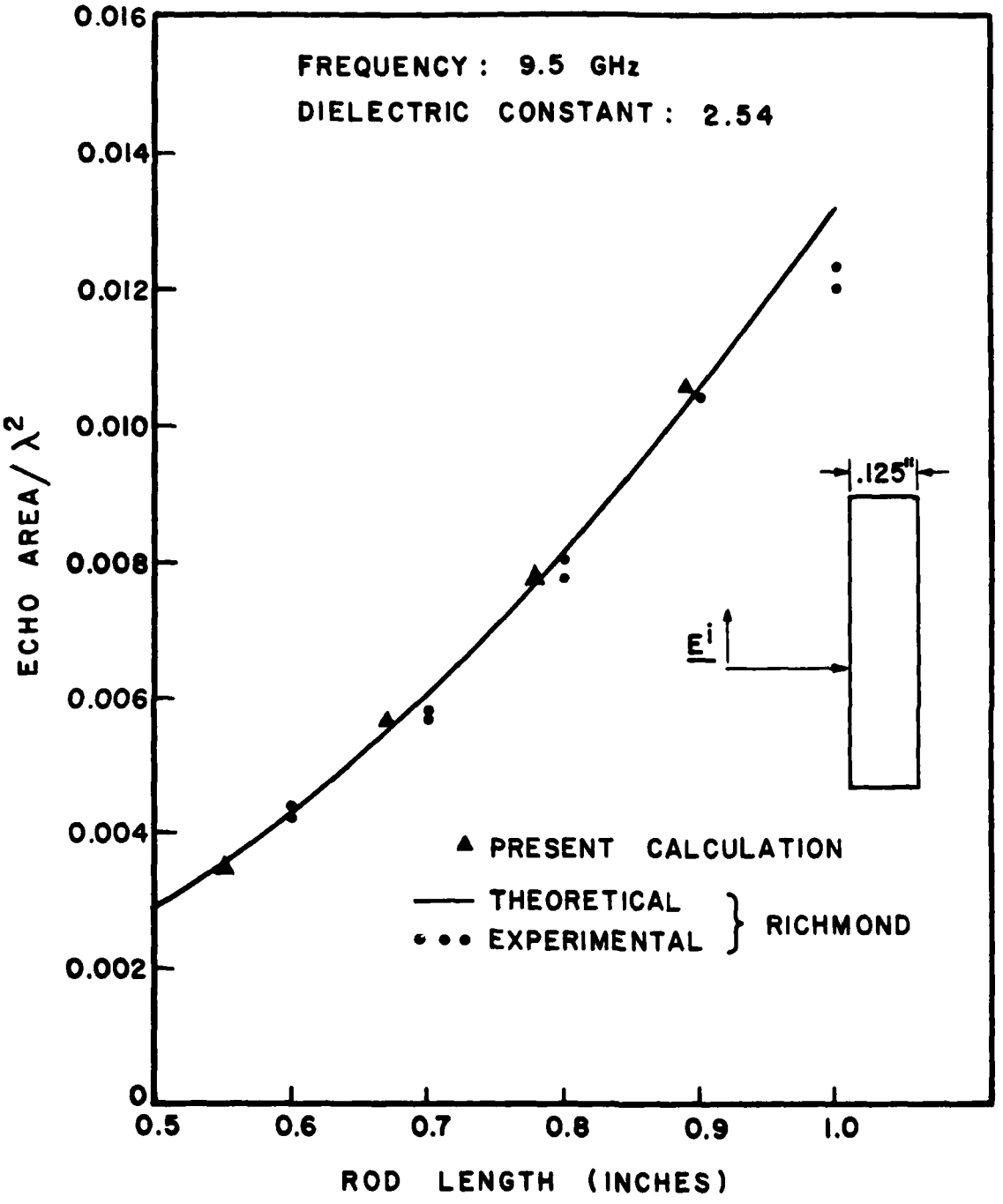

Figure 17. Comparison between the calculated results and Richmond's data for a dielectric cylinder.

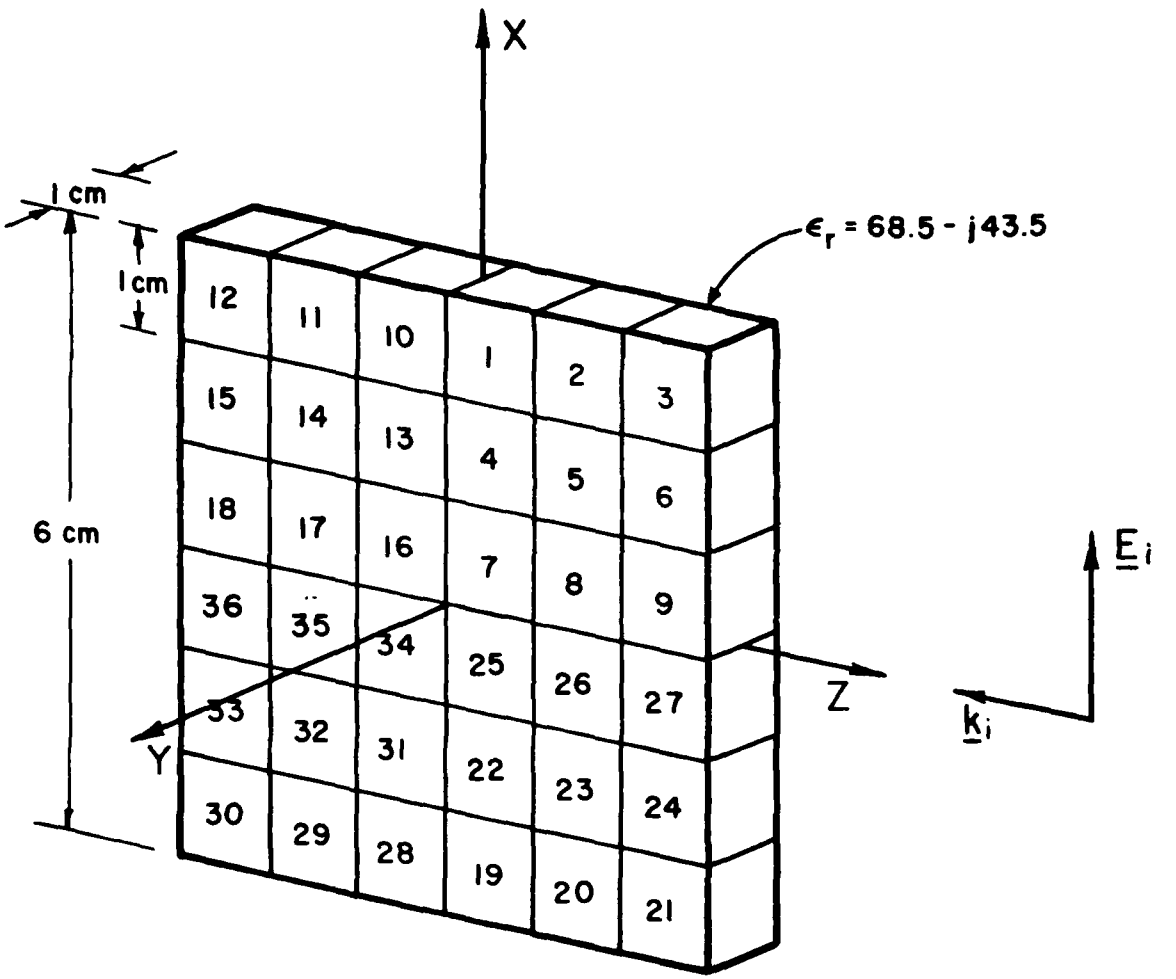

Figure 18. A rectangular box of saline water under plane wave excitation (numbers are the index numbers for the volume cells).

TABLE III

ELECTRIC FIELD DISTRIBUTION IN THE 36-CELL RECTANGULAR BLOCK

E_x - DISTRIBUTION IN THE 36-CELL RECTANGULAR BLOCK

CELL NO.	PRESENT CALCULATION	MICHIGAN STATE	
		CALCULATED	MEASURED
1	.0510	.0518	.0518
2	.0600	.0573	.0523
3	.0952	.0976	.1632
4	.0816	.0862	.0862
5	.0883	.0827	.0832
6	.1040	.1090	.2355
7	.0870	.0935	.0935
8	.1225	.1180	.1180
9	.1355	.1410	.2869
10	.0292	.0339	.0459
11	.1008	.1050	.0878
12	.1611	.1570	.2017
13	.0930	.1020	.1258
14	.1956	.2020	.2020
15	.2546	.2480	.1256
16	.1345	.1460	.1460
17	.2267	.2330	.2330
18	.3294	.3220	.5410

TABLE III (Continued)

E_z - DISTRIBUTION IN THE 36-CELL RECTANGULAR BLOCK

CELL NO.	PRESENT CALCULATION	MICHIGAN STATE	
		CALCULATED	MEASURED
1	.2127	.2140	.2167
2	.1719	.1710	.1647
3	.1326	.1310	---
4	.0982	.0963	.0963
5	.0955	.0927	.0927
6	.0730	.0698	---
7	.0930	.0991	.0925
8	.0723	.0783	.0820
9	.0325	.0364	---
10	.2207	.2230	.2230
11	.1355	.1360	.1456
12	.0554	.0544	---
13	.0666	.0626	.0626
14	.0330	.0328	.0344
15	.0342	.0348	---
16	.0964	.1010	.1010
17	.0932	.0963	.0963
18	.0543	.0563	---

TABLE III (Continued)

E_t – DISTRIBUTION IN THE 36-CELL RECTANGULAR BLOCK

CELL NO.	PRESENT CALCULATION	MICHIGAN STATE	
		CALCULATED	MEASURED
1	.2187	.2202	---
2	.1821	.1803	---
3	.1633	.1633	---
4	.1277	.1292	---
5	.1301	.1242	---
6	.1271	.1294	---
7	.1274	.1362	---
8	.1422	.1416	---
9	.1394	.1456	---
10	.2226	.2256	---
11	.1689	.1718	---
12	.1703	.1662	---
13	.1144	.1137	---
14	.1984	.2047	---
15	.2569	.2505	---
16	.1655	.1775	---
17	.2451	.2521	---
18	.3339	.3269	---

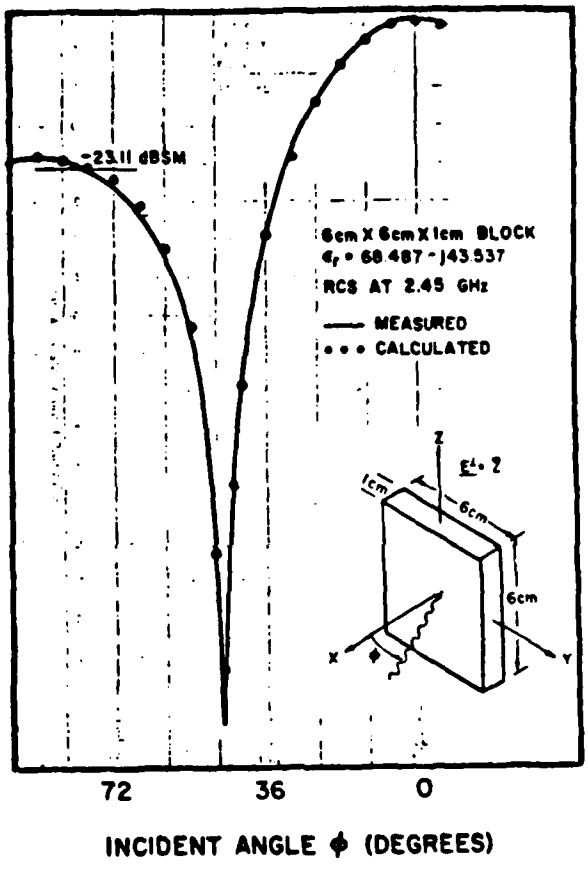

Figure 19. Comparison between calculated and measured RCS of square boxes of saline water shown in Figure 18.

Figure 20 shows an I-shaped box of saline water under plane wave excitation. The numbers are the index number for the volume cells. Tables 4a, 4b and 4c show the calculated x,y and total fields inside the I-shaped box of saline water. The agreements between the present calculation and that at Michigan State University [36] are good. Figure 21 shows the comparison between the measured and calculated back-scatter cross section data generated at Georgia Tech. The disagreement could be partially due to the acrylic box as indicated in the figure. Good agreements with Michigan State data were observed also for three other cases, including a cube and two rectangular cylinders, which will not be presented here.

Computations were also made for the dielectric sphere. Figure 22 shows the back-scatter cross section of a dielectric sphere with a relative permittivity of 2.592. The results deteriorate as Ka becomes greater than 2. Figures 23 and 24 show the computed results for a dielectric sphere with a complex dielectric constant of 29.43-j0.158 using 128-cell and 232-cell, respectively. The results are rather disappointing when compared with data generated by Burr and Lo [40], as shown in Figures 23 and 24. The resonance frequencies were shifted by 20 percent and the resonance peaks are off by 30 percent. This failure in predicting resonance phenomena in a dielectric sphere by the volume integral equation approach is in contrast to the high accuracy achieved for the calculation of conducting spheres by a surface integral equation approach [41,42]. To explain the lack of adequate accuracy in predicting resonances, we observe that the point-matching is enforced at the center of the volume cells -- not at the surface of the scatterer. Since the resonance is very sensitive to the physical size and shape of the object, the failure to project the accurate size of the object in the computation may be a source of error. Even more puzzling is that this situation should lead to reduction in apparent size and shift up the resonance peaks to about ka = 0.63 and ka = 0.84 in Figure 24, instead of lowering them to 0.52 and 0.72, respectively.

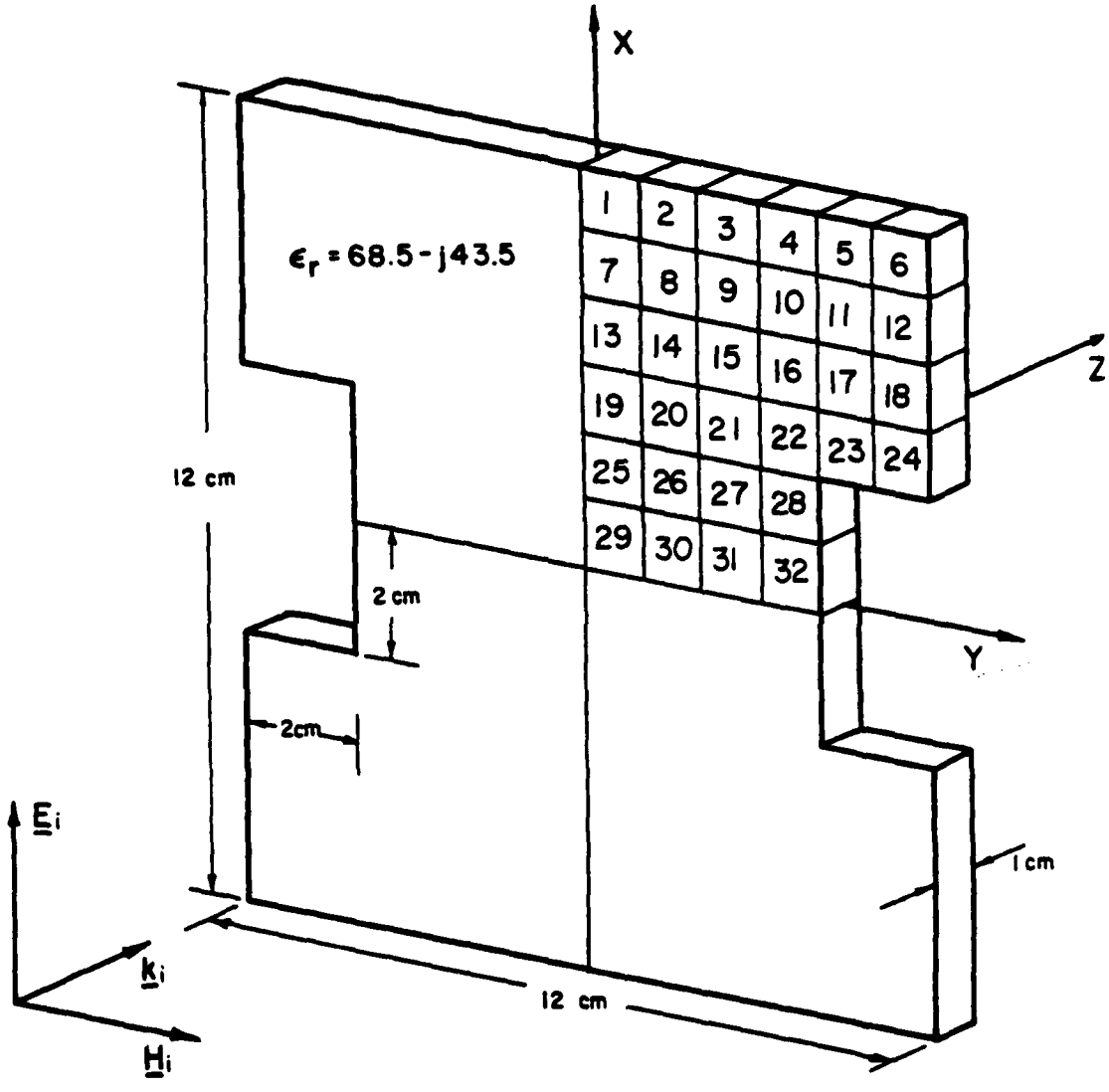

Figure 20. An I-shaped box of saline water under plane wave excitation (numbers are the index numbers for the volume cells).

TABLE IV

ELECTRIC FIELD DISTRIBUTION IN THE 128-CELL BLOCK

E_x-DISTRIBUTION IN THE 128-CELL BLOCK

CELL NO.	PRESENT CALCULATION	MICHIGAN STATE	
		CALCULATED	MEASURED
1	.0545	.0573	---
2	.0342	.0353	---
3	.0656	.0676	---
4	.0279	.0294	---
5	.0906	.0879	---
6	.0899	.0887	---
7	.0787	.0807	---
8	.0557	.0558	---
9	.1028	.1071	---
10	.0165	.0173	---
11	.1103	.1057	---
12	.1027	.1018	---
13	.0775	.0769	.0770
14	.0681	.0681	.0681
15	.0967	.1017	.1017
16	.0393	.0386	.0518

TABLE IV (Continued)

E_x-DISTRIBUTION IN THE 128-CELL BLOCK

CELL NO.	PRESENT CALCULATION	MICHIGAN STATE	
		CALCULATED	MEASURED
17	.0905	.0853	.0915
18	.0940	.0941	.0766
19	.0562	.0567	---
20	.0544	.0575	---
21	.0493	.0517	---
22	.0951	.0982	---
23	.0656	.0611	---
24	.0838	.0823	---
25	.0426	.0421	---
26	.0623	.0665	---
27	.0465	.0431	---
28	.1440	.1494	---
29	.0633	.0617	.0617
30	.0651	.0695	.0739
31	.0696	.0661	.0661
32	.1834	.1887	.0766

TABLE IV (Continued)

E_y-DISTRIBUTION IN THE 128-CELL BLOCK

CELL NO.	PRESENT CALCULATION	MICHIGAN STATE	
		CALCULATED	MEASURED
1	.0228	.0239	---
2	.0482	.0501	---
3	.0467	.0424	---
4	.0698	.0623	---
5	.0743	.0681	---
6	.0497	.0466	---
7	.0309	.0303	---
8	.0867	.0858	---
9	.1254	.1256	---
10	.1215	.1234	---
11	.0892	.0912	---
12	.0490	.0500	---
13	.0197	.0192	.0243
14	.0450	.0420	.0316
15	.0496	.0423	.0423
16	.0565	.0486	.0486

TABLE IV (Continued)

E_y-DISTRIBUTION IN THE 128-CELL BLOCK

CELL NO.	PRESENT CALCULATION	MICHIGAN STATE	
		CALCULATED	MEASURED
17	.0713	.0671	.0547
18	.0567	.0544	---
19	.0170	.0162	---
20	.0512	.0485	---
21	.0957	.0937	---
22	.1370	.1382	---
23	.1482	.1506	---
24	.1131	.1136	---
25	.0299	.0296	---
26	.0658	.0641	---
27	.0580	.0544	---
28	.0304	.0262	---
29	.0164	.0162	.0194
30	.0375	.0369	.0371
31	.0355	.0344	.0344
32	.0165	.0157	---

TABLE IV (Continued)

E_t-DISTRIBUTION IN THE 128-CELL BLOCK

CELL NO.	PRESENT CALCULATION	MICHIGAN STATE	
		CALCULATED	MEASURED
1	.05906	.06208	---
2	.05910	.06123	---
3	.08048	.07979	---
4	.07517	.06709	---
5	.11720	.11119	---
6	.10280	.10019	---
7	.08449	.08627	---
8	.10300	.10235	---
9	.16220	.16500	---
10	.12270	.12460	---
11	.14180	.13961	---
12	.11380	.11342	---
13	.07995	.07926	---
14	.08163	.08001	---
15	.10870	.11015	---
16	.06883	.06206	---

TABLE IV (Continued)

E_t-DISTRIBUTION IN THE 128-CELL BLOCK

CELL NO.	PRESENT CALCULATION	MICHIGAN STATE	
		CALCULATED	MEASURED
17	.11520	.10853	---
18	.10980	.10869	---
19	.05870	.05897	---
20	.07472	.07522	---
21	.10760	.10702	---
22	.16680	.16954	---
23	.16210	.16252	---
24	.14080	.14030	---
25	.05210	.05146	---
26	.09062	.09236	---
27	.07433	.06940	---
28	.14720	.15167	---
29	.06537	.06379	---
30	.07588	.07870	---
31	.07810	.07450	---
32	.18410	.18940	---

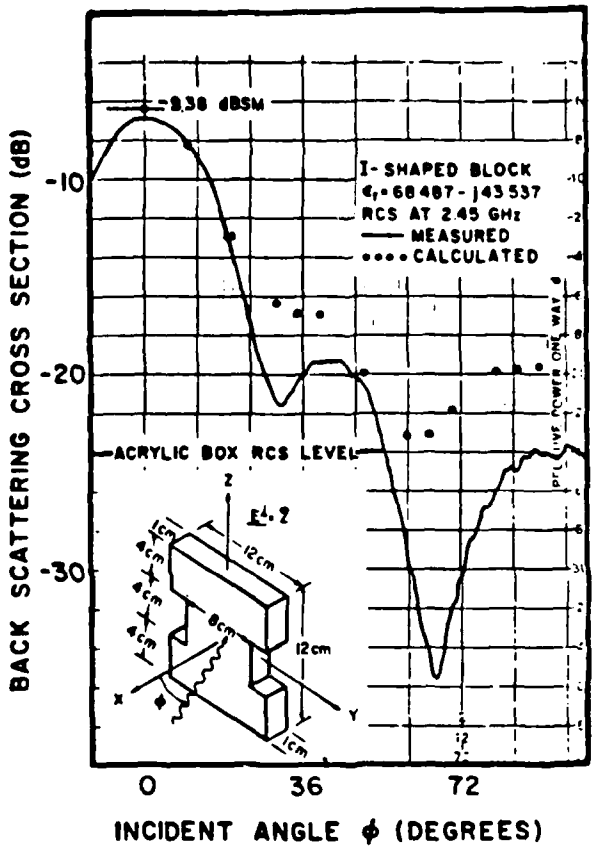

Figure 21. Comparison between calculated and measured RCS of I-shaped boxes of saline water.

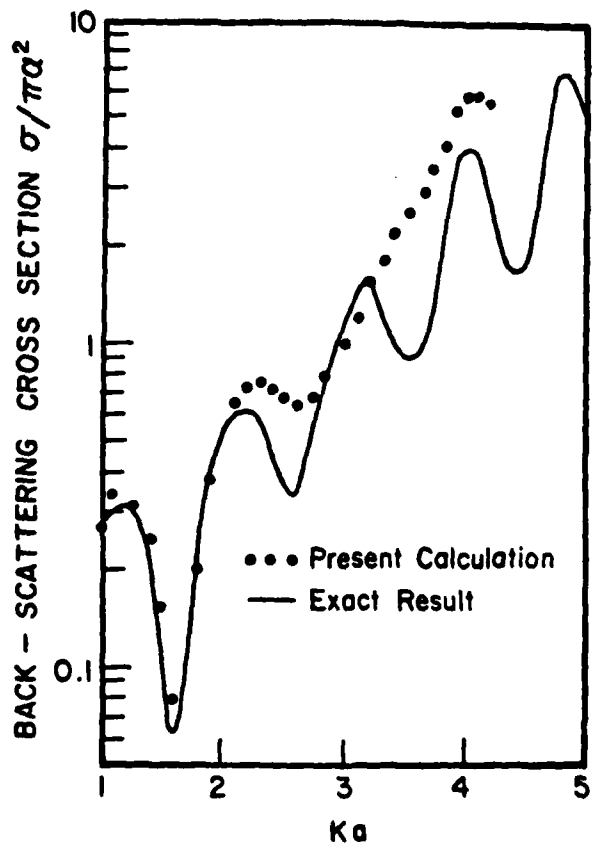

Figure 22. Calculation of RCS of a sphere with a dielectric constant of 2.592 as a function of radius a.

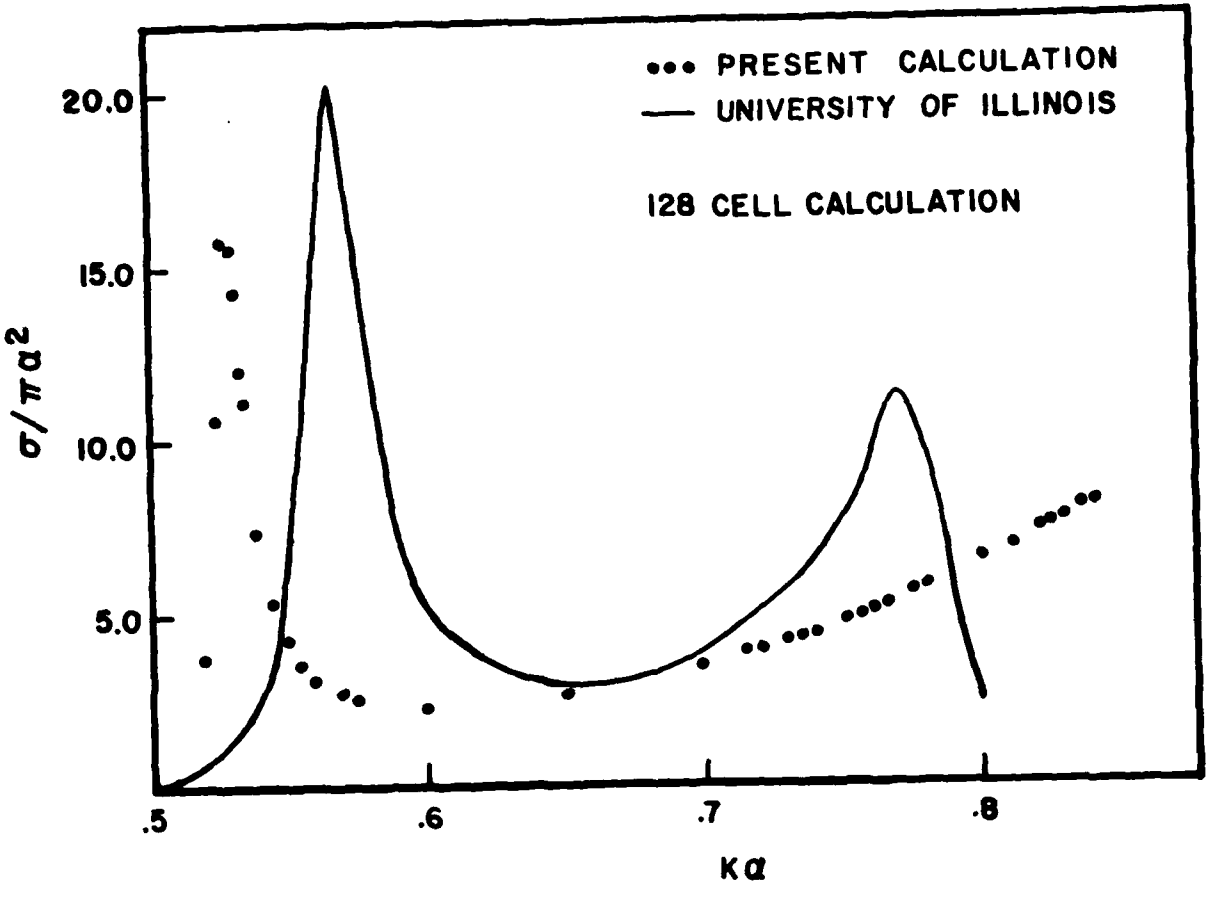

Figure 23. Calculation of back-scatter cross-section for a sphere of radius a and $\epsilon_r = 29.43 - j0.158$.

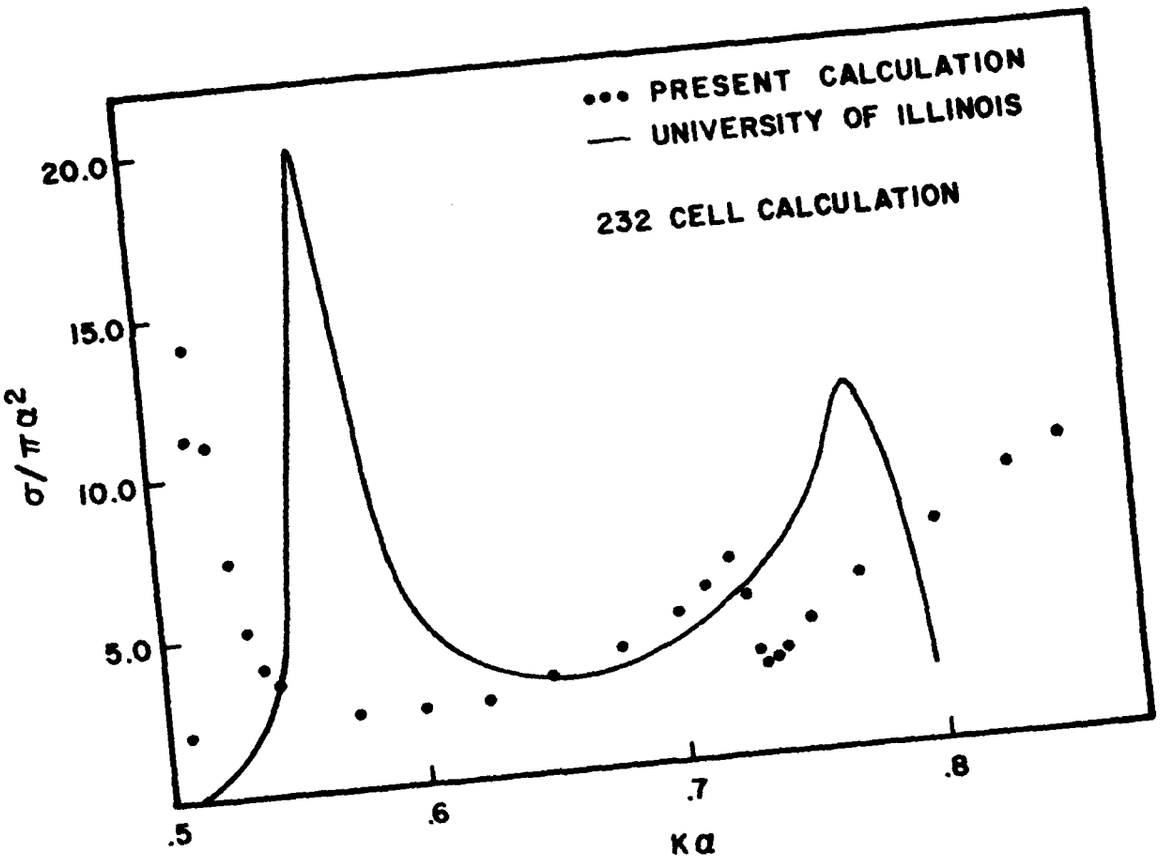

Figure 24. Calculation of back-scatter cross-section for a sphere of radius a and $\varepsilon_r = 29.43 - j0.158$.

On the other hand, the computational accuracy may be improved by using more volume cells -- subject, of course, to the limitation of the central memory size of the computer being used. This is indicated in Figures 23 and 24, in which it is shown that the second resonance appears after the number of volume cells is increased from 128 to 232.

B. Scattering Computation for 1-foot birds

The Green Wingtail, which is an important migrant bird, was selected for extensive measurement and computation. This bird is typically 14.75 to 15.50 inches and weighs about a pound. At 1 GHz this bird is about 1 wavelength in length. Figures 14 and 15 show plaster-of-paris models for a Green Wingtail in sitting and flight positions, respectively.

Four simulation models, SB1 through SB4, were generated in this project. For the first three models, a number of problems developed in the experimental work. The permittivity was too high or too low or not uniform. These difficulties and the unsatisfactory data for the sphere directed the computation toward a more conservative approach. It was then decided that measurement for the bird should be started with a smaller bird exactly as the numerical model made of a group of cubic volume cells. With this principle in mind, SB4 was fabricated. Figure 25 shows the print-out of the cell centers for the side, front and top views for SB4. Figure 26 shows the geometry of the coordinate system and a plane wave incident in the x-z plane, which is the plane of symmetry for the bird. Figures 27 and 28 show fair agreement between the computed and measured results. It is noticed that the agreement is good as long as there is no sharp variation in the pattern. This difficulty in predicting sharp field variation and resonance phenomena may explain the use of specific absorption rate (SAR) in dealing with dielectric scattering problems [38].

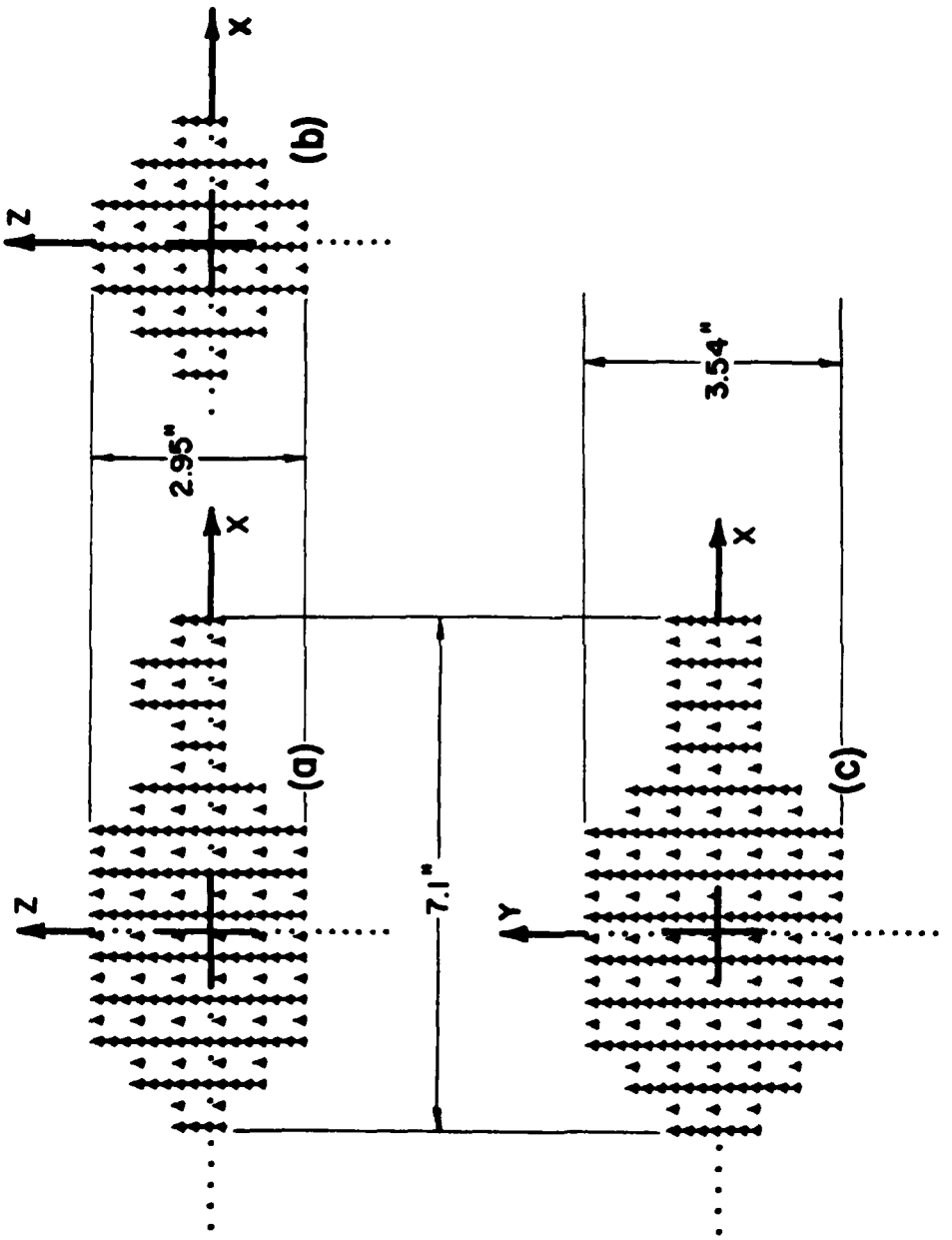

Figure 25. Side(a), front(b), and top(c) views of the 118 cell bird no. SB-4 to simulate a 0.8 pound Green-Winged Teal, $\varepsilon_r = 47.0 - j13.2$.

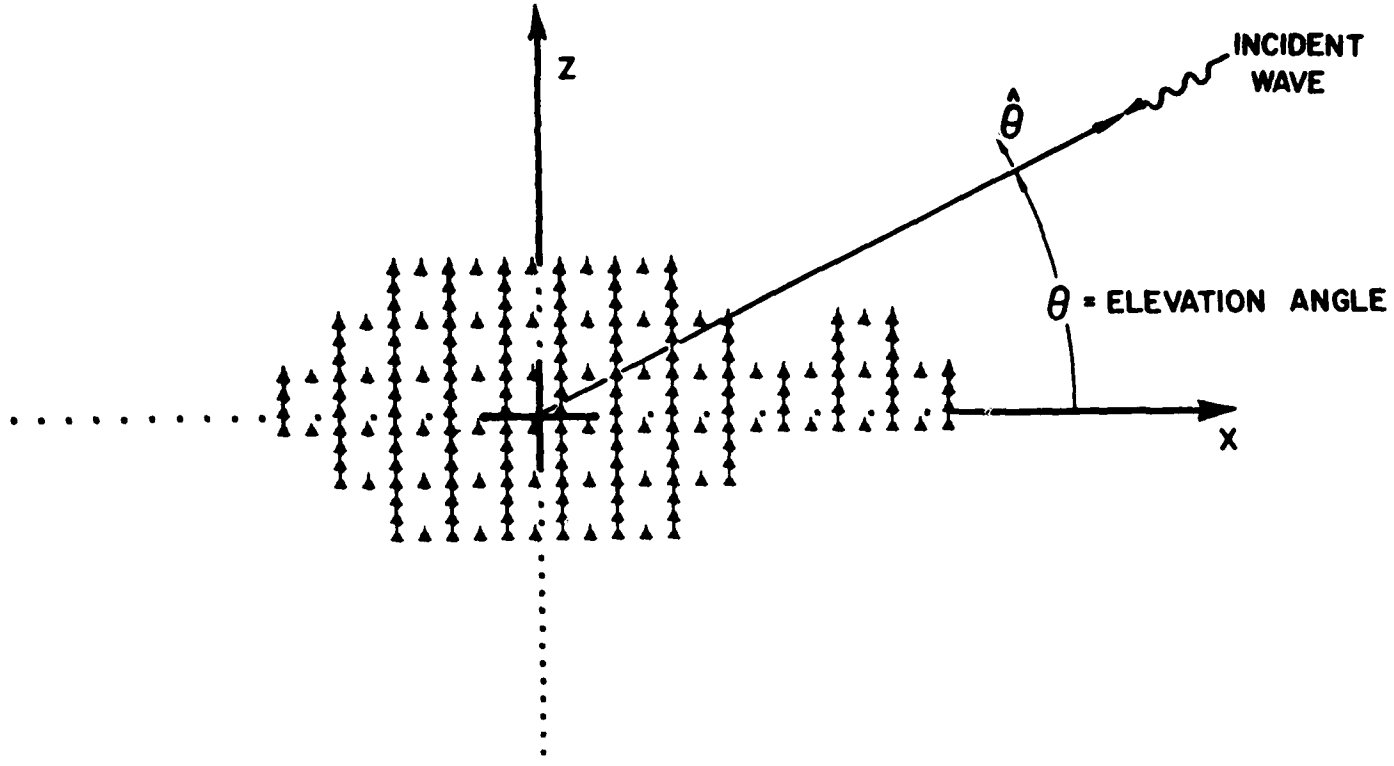

Figure 26. Simulated bird model SB4 under plane wave excitation.

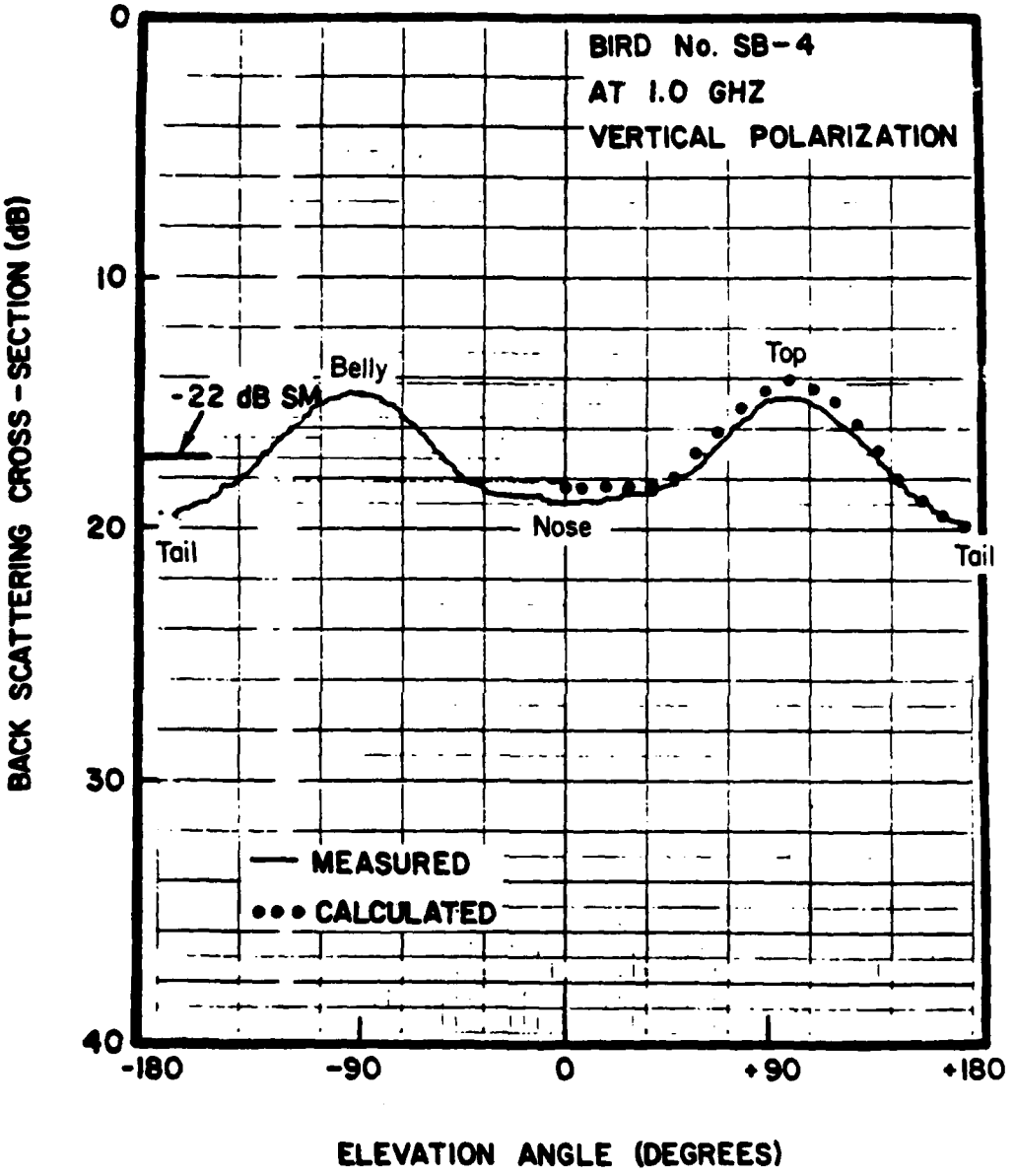

Figure 27. Back scattering cross section of bird SB4 versus elevation angle $\hat{\theta}$ with vertical polarization as shown in Figures 25 and 26.

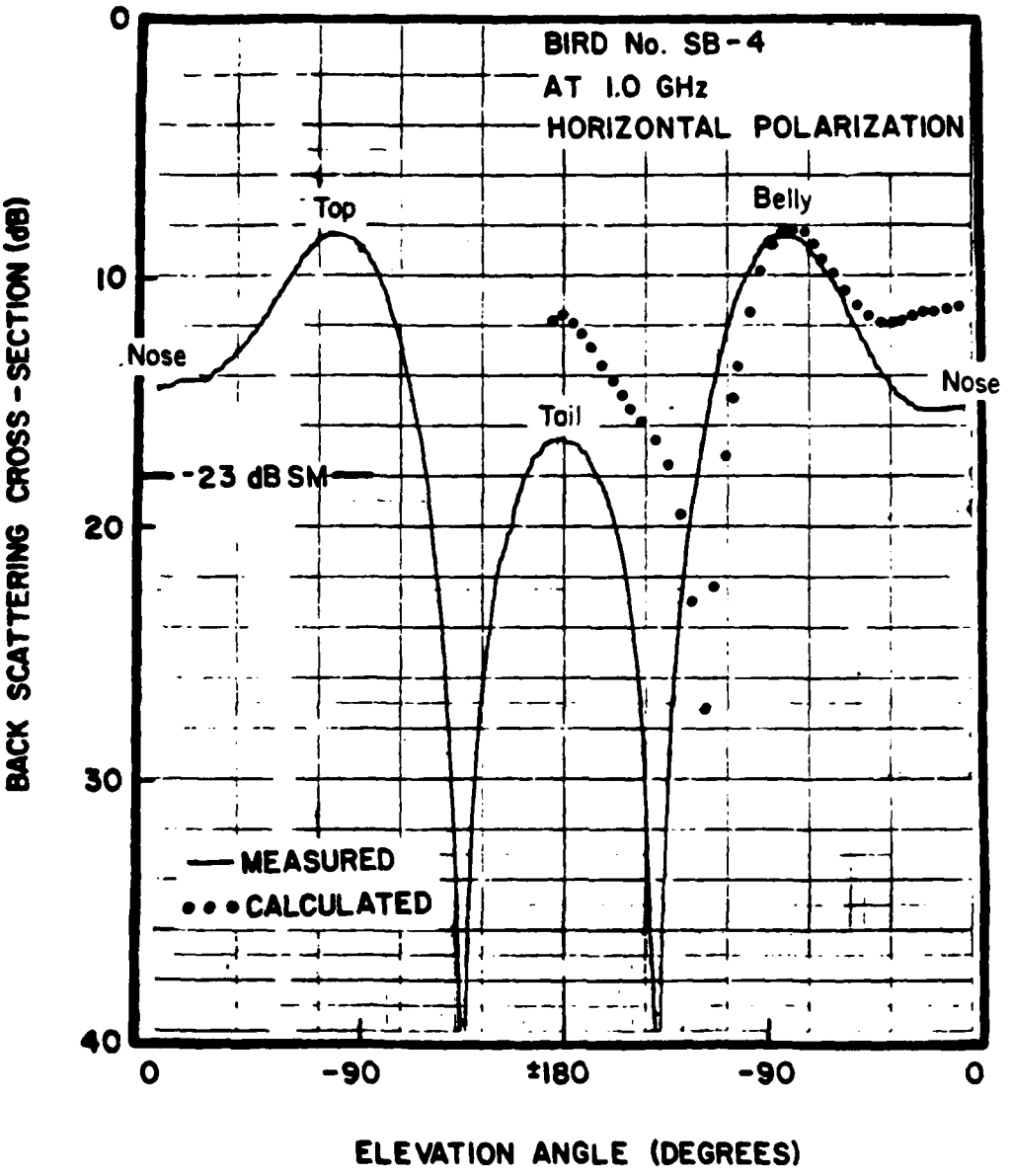

Figure 28. Back scattering cross section of bird SB4 versus elevation angle θ with horizontal polarization as shown in Figures 25 and 26.

SECTION V

IMPROVEMENTS OF COMPUTER ALGORITHM

A number of modifications have been made on the existing Georgia Tech volume integral equation algorithm to make it more efficient for the computation of dielectric scatterers. Major improvements included: (1) the reduction of execution time and central memory requirement by 50% by using symmetrical matrices, and (2) the reduction of execution time and central memory requirement by 75% for scattering problems with one-plane symmetry and by 87.5% for scatterers with two-plane symmetry. In addition, the banded matrix [43,44] and virtual memory [45] techniques have been implemented successfully for small scatterers.

A. Symmetrical Matrices

It can be shown that the matrix of the volume integral equation algorithm is symmetrical if the following conditions are satisfied.

(1) the dielectric body is homogeneous and has a constant permittivity,

(2) the volume cells are equal in size,

(3) the volume cells are identical in shape.

The third condition is not critical and can often be ignored. To prove this, one can examine the following matrix elements in the algorithm

$$Z_{pk}^{\ell n} = \int - j\omega u_o \left[\delta_n^k + \frac{1}{k_o^2} \frac{\partial^2}{\partial u_n \partial u_k}\right] \frac{e^{-jk_o|\underline{r}_p - \underline{r}'|}}{4\pi|\underline{r}_p - \underline{r}'|} B_\ell^k(\underline{r}')\, d\underline{r}'$$

$$- \frac{\varepsilon_r(\underline{r}_p) + 2}{3j\omega[\varepsilon(\underline{r}_p) - \varepsilon_o]} \delta_k^n \delta_p^\ell \qquad (43)$$

and

$$Z_{\ell n}^{pk} = \int - j\omega u_o \left[\delta_k^n + \frac{1}{k_o^2} \frac{\partial^2}{\partial u_k \partial u_n}\right] \frac{e^{-jk_o|\underline{r}_\ell - \underline{r}'|}}{4\pi|\underline{r}_\ell - \underline{r}'|} B_p^n(\underline{r}')\, d\underline{r}'$$

$$- \frac{\epsilon_r(\underline{r}_\ell) + 2}{3j\omega[\epsilon(\underline{r}_\ell)-\epsilon_o]} \delta_n^k \delta_\ell^p \qquad (44)$$

where $k,n = 1,2,3$ or x,y,z

$\ell,p = 1,2,....L$; the index number of volume cell,

δ_n^k = the Kronecker delta function,

B_ℓ^k = a pulse function being unity in the ℓth volume cell associated with k (which designates x,y or z and is merely a dummy index number of no consequence to the integration).

Since the pulse function B_p^n restricts the domain of integration to the unit volume, cell ℓ in Equation (43) and cell p in Equation (44), $|\underline{r}_p-\underline{r}'|$ and $|\underline{r}_\ell-\underline{r}'|$ are equal. Thus $Z_{pk}^{\ell n}$ and $Z_{\ell n}^{pk}$ are equal under the three conditions stated.

For a symmetrical matrix, there are standard subroutines to handle its inversion or solution. The improved Georgia Tech algorithm is given an acronym "BPWSM" to denote "Biological-Plane-Wave-Symmetrical-Matrix". This algorithm has been successfully applied in a number of cases with a resulting 50% reduction in computer central memory and execution time.

B. Symmetrical Scatterers

Two improved algorithms, BHPW2 and BHPW4, have been completed to handle scattering problems with one-plane and two-plane symmetries with resulting reductions of 75% and 87.5% in computer time and central memory, respectively. These are discussed separately as follows.

(1) Scattering problems with one-plane symmetry (BHPW2)

When the direction of propagation of an incident plane wave is in the plane of symmetry of a conducting scatterer, it is recognized that some symmetric behavior must exist in the induced current on the surface of the scatterer. Without loss of generality, Cartesian coordinates can be set up so that the plane of symmetry coincides with the XZ plane as shown in Figure 29. The polarization

of the incident wave is assumed to be either parallel or perpendicular to the XZ plane. Arbitrary polarization can be decomposed into two components, one parallel and the other perpendicular to the XZ plane. The overall scattering problem can then be treated by superposing the fields due to these two component incident fields.

At two symmetrical points ℓ and $\ell + L/2$ in Figure 29, the components of the induced currents exhibit the following relationships

$$J_\ell^x = J_{\ell + L/2}^x \quad ,$$

$$J_\ell^y = -J_{\ell + L/2}^y \quad ,$$

$$J_\ell^z = J_{\ell + L/2}^z \quad , \tag{45}$$

when the incident $\underline{E}^i$ is parallel to the z-axis. In Equation (45), J_ℓ^x denotes, for example, the x component of the induced current in the ℓth cell.

When the incident $\underline{E}^i$ is parallel to the y-axis, the induced current on the scatterer has the following property

$$J_\ell^x = -J_{\ell + L/2}^x \quad ,$$

$$J_\ell^y = J_{\ell + L/2}^y \quad ,$$

$$J_\ell^z = -J_{\ell + L/2}^z \quad . \tag{46}$$

The matrix equation to be solved is

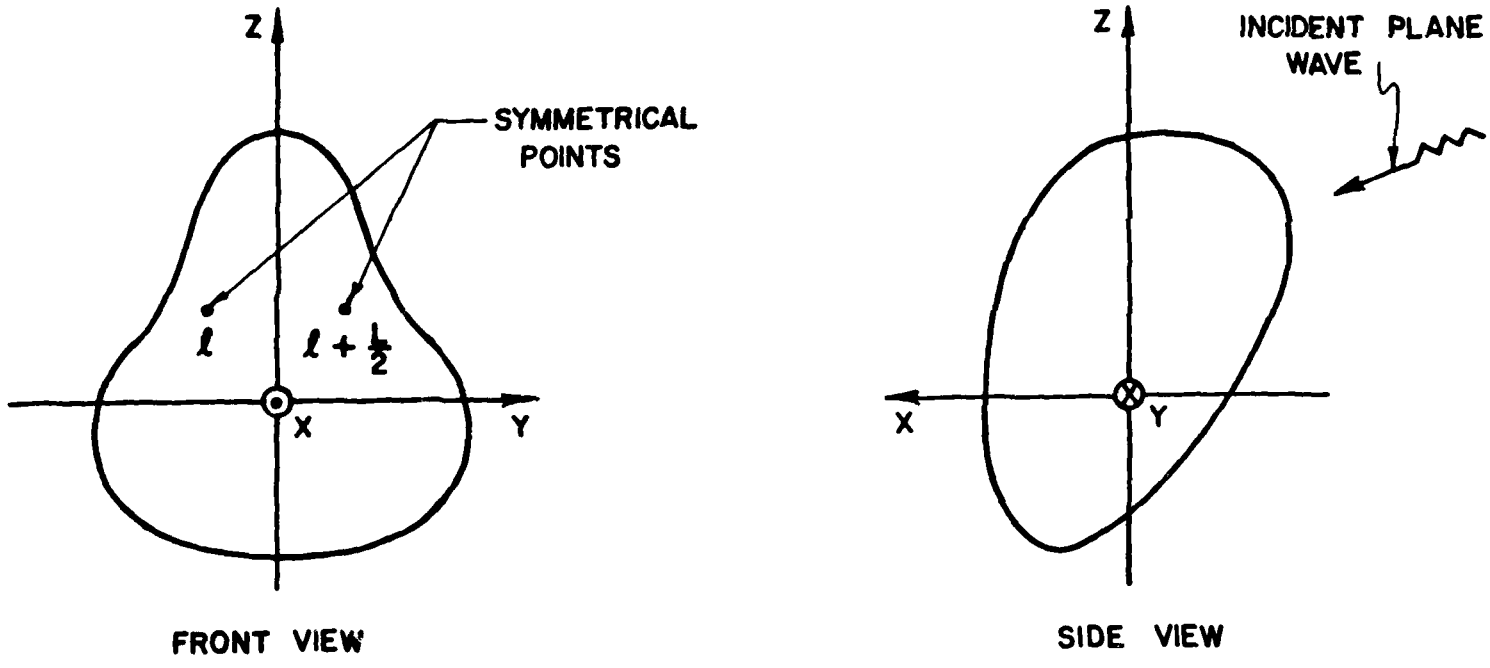

Figure 29. A symmetrical scatterer illuminated by a plane wave incident in the plane of symmetry.

$$\sum_{\ell=1}^{1} \sum_{k=1}^{3} J_{\ell}^{k} \; Z_{pk}^{\ell n} = V_{p}^{n} \qquad (47)$$

$n=1,2,3$

$p=1,\ldots L.$

Since the excitation is symmetrical, we have

$$V_{\ell}^{n} = V_{\ell}^{n} + L/2 \qquad (48)$$

Substitution of Equations (45) and (48) into Equation (47) yields

$$\sum_{k=1}^{L/2} \sum_{k=1}^{3} J_{\ell}^{k} [\, Z_{pk}^{\ell n} + Z_{pk}^{(L/2+\ell)n} (-1)^{k+1}] = V_{p}^{n} \,, \qquad (49)$$

$n=1,2,3$

$p=1,2,\ldots L/2$

for $\underline{E}^{i} = \hat{z}$

Substitution of Equation (46) and (48) into Equation (47) yields

$$\sum_{\ell=1}^{L/2} \sum_{k-=1}^{3} J_{\ell}^{k} [Z_{pk}^{\ell n} + Z_{pk}^{(L/2+\ell)n} (-1)^{k}] = V_{p}^{n} \qquad (50)$$

$n=1,2,3$

$p=1,2,\ldots L/2$

for $\underline{E}^{i} = \hat{y}$

Equations (49) and (50) show that the number of equations has been reduced from 3L to 3(L/2).

(2) two-plane symmetry

Figure 30 shows a scattering problem symmetrical with respect to the x-z and y-z planes. The directive of propagation of a plane wave is assumed to be parallel to the z-axis. When $\underline{E}^i = \hat{z}$, we have

$$\begin{cases} J_x^1 = J_x^2 = J_x^3 = J_x^4 \\ J_y^1 = -J_y^2 = -J_y^3 = J_y^4 \\ J_z^1 = J_z^2 = J_z^3 = J_z^4 \end{cases} \quad . \tag{51}$$

When $\underline{E}^i = \hat{y}$, we have

$$\begin{cases} J_x^1 = J_x^2 = -J_x^3 = -J_x^4 \\ J_y^1 = J_y^2 = J_y^3 = J_y^4 \\ J_z^1 = -J_z^2 = -J_z^3 = J_z^4 \end{cases} \tag{52}$$

In addition, the excitation at cells 1,2,3 and 4 are identical. The number of Equations in Equation (49) can therefore be reduced to one-quarter of its original size as follows

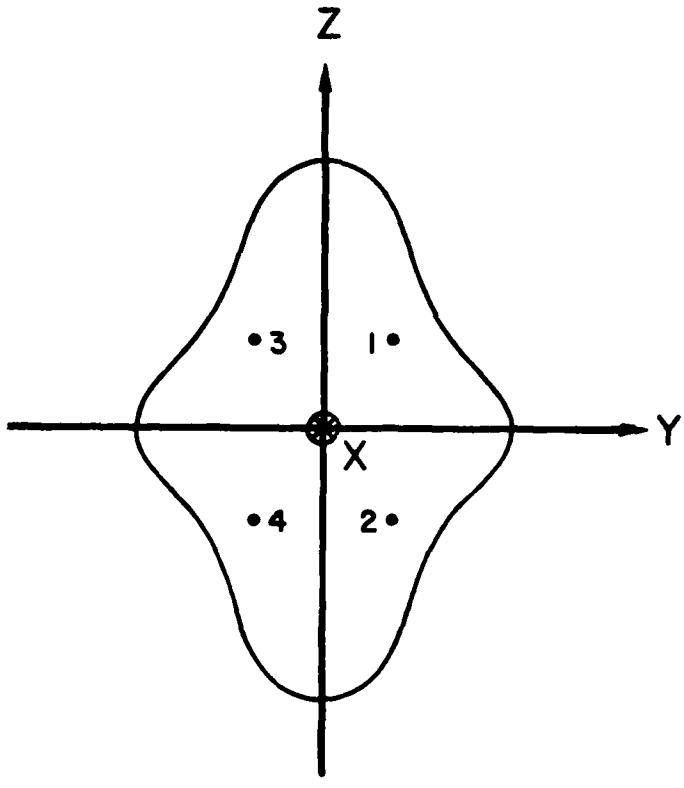

Figure 30. A scattering problem with two-plane symmetry.

$$\sum_{\ell=1}^{L/4} \sum_{k=1}^{3} J_\ell^k \left\{ Z_{pk}^{\ell n} + (-1)^{k+1} \left[Z_{pk}^{(L/4+\ell)m} + Z_{pk}^{(L/2+\ell)n} \right] + \right.$$

$$\left. + Z_{pk}^{(3/4\ L+\ell)n} \right\} = V_p^n \qquad (53)$$

$$n = 1,2,3$$

$$p = 1,2, \ldots, L/4$$

when $\underline{E}^i = \hat{z}$.

Substitution of Equations (52) into Equation (47) yields

$$\sum_{\ell=1}^{L/4} \sum_{k=1}^{3} J_\ell^k \left\{ Z_{pk}^{\ell n} + (-1)^{k(1-\delta_{1k})} Z_{pk}^{(L/4+\ell)n} + (-1)^{k(1-\delta_{zk})} Z_{pk}^{(L/2+\ell)n} + \right.$$

$$\left. + (-1)^{k(1-\delta_{3k})} Z_{pk}^{(3/4\ L+\ell)n} \right\} = V_p^n \qquad (54)$$

$$n = 1,2,3$$

$$p = 1,2, \ldots, L/4$$

when $\underline{E}^i = \hat{y}$. In Equations (54) δ_{ju} is the Kronecker delta.

C. Banded Matrix Techniques

The banded matrix technique has been previously employed by Ferguson, et al. [43] and Balestri, et al. [44] in the scattering and radiation of thin-wire structures. These authors have demonstrated that the banded matrix technique can reduce the computer execution time in the computation of thin-wire scattering and radiation involving small matrices. They also demonstrated that wire-grid problems involving more wire segments than can be managed in the computer central memory can be solved by the banded matrix technique after proper numbering of wire segments. The segments are

numbered such that the difference between segment numbers for all neighboring segment pairs is small as compared with the total number of segments. In this case the large matrix elements are kept close to the principal diagonal of the matrix.

The basic banded matrix technique has been applied to the Volume Integral Equation algorithm. However, there are three unknowns in the nth cell in the Volume Integral Equation approach, while there is only one unknown in the nth segment in the wire algorithm. Fortunately the matrix generated in the Volume Integral Equation algorithm has a tendency to be banded. Figure 31 shows the matrix for the case of a simple cylinder formed with a linear array of volume cells. It can be seen that a diagonal band extended to one third of the columns and the rows must be included in order to include all the nonzero elements. It is also noted that outside this band all the matrix elements are zero. This phenomenon is due to the lack of coupling between orthogonal components of the electromagnetic source and field. For an object of more complex geometry, such as a sphere, elements throughout the entire matrix can be nonzero except for those related to the coupling between orthogonal components in the self cell. Figure 32 shows the matrix for the case of a prolate spheroid of 12 cells, which is weakly banded with some nonzero elements away from the diagonal band.

We now define the normalized width of the diagonal band as

$$\text{Normalized Width of diagonal band} = [(\text{number of rows in band}) + (\text{number of columns in band})]\,[(\text{total number of rows}) \times 2] \quad (55)$$

Numerical tests have been conducted to explore the convergence of the solutions as a function of the normalized width of the diagonal band. Figure 33 shows that the error in the solution is reduced as the width of the diagonal band is increased. The error falls to near zero when the normalized width of the diagonal band is only 0.6. Note that for a general matrix the error reaches zero when the normalized width of the diagonal band approaches unity. It is also noteworthy that the error is only 5% when the normalized width of the diagonal is 0.15 or larger. Thus, a

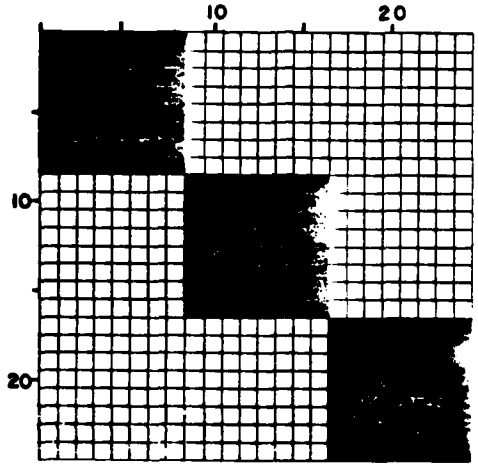

Note: ◘ The size of the shaded area in the square cell is proportional to the magnitude of the matrix element.

Figure 31. **A display of the magnitude of matrix elements in a VIE matrix for an 8-cell dielectric cylinder which is strongly banded.**

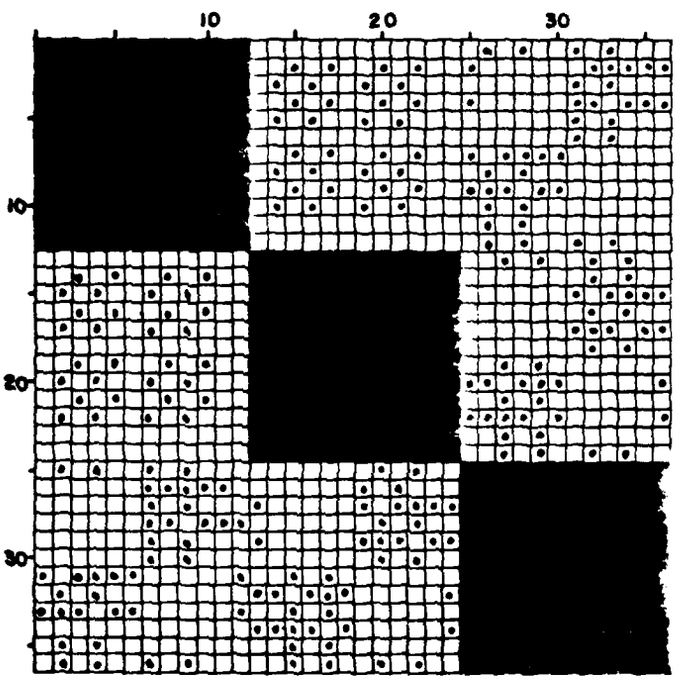

Note: ⊡ The size of the shaded area in the square cell is proportional to the magnitude of the matrix element.

Figure 32. A display of the magnitude of matrix elements in a VIE matrix for a 12-cell prolate spheroid which is weakly banded.

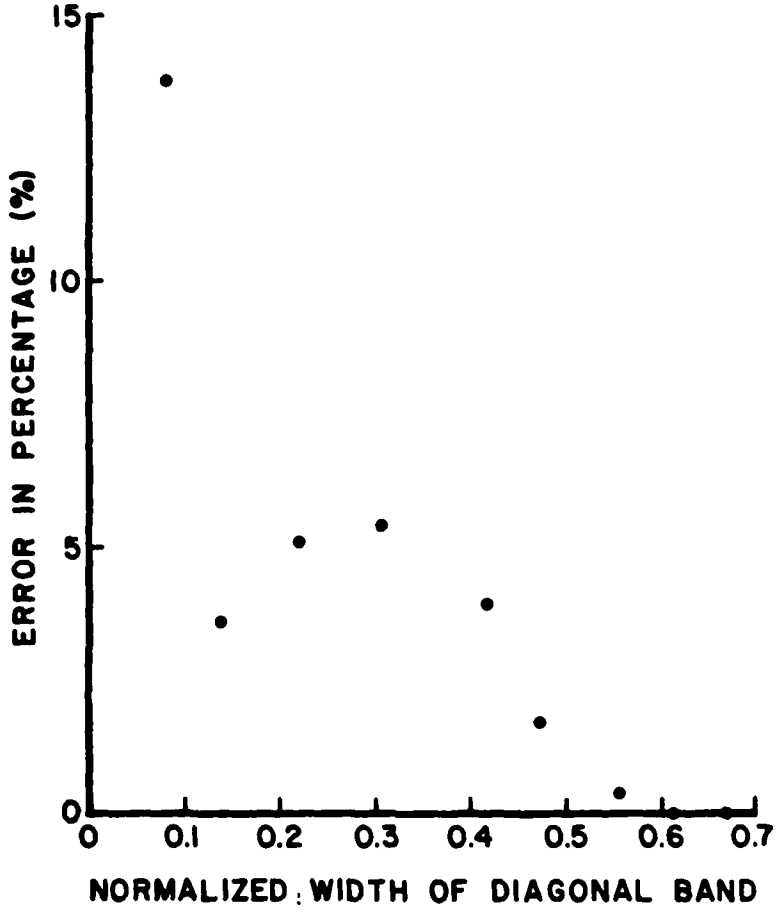

Figure 33. Convergence of solution for the case of a 12-cell prolate spheroid expressed in percentage of error as a function of the normalized width of diagonal band.

significant reduction of execution time can be accomplished for a small scatterer. These numerical tests also strongly indicate that a large scatter, which can not be handled in the computer central memory, may be treated using the banded matrix technique.

D. Virtual Memory Techniques

The virtual memory is a software technique, in contrast to the extended-memory hardware capability, to store data in a digital computer for rapid and efficient access in computer-aided numerical analyses to overcome the limitations imposed by the size of the computer central memory. The basic algorithm had been developed by Carbrey [45] for real-valued data, and was employed in the present research to expand the capability of the Volume Integral Equation algorithm to handle large dielectric scatterers. When using exclusively the computer central memory to handle the matrix in the computation, the CDC CYBER-74 computer at Georgia Tech can only deal with matrices of about 38,300 complex elements, or about 65 volume cells. The use of the virtual memory technique can potentially make it possible to handle a matrix with 4×10^6 complex elements, or 660 volume cells, which is about ten times the size of those limited by the computer central memory. A serious disadvantage of the virtual memory technique is its extremely large execution time, often ten times more than methods using central core memory alone.

The tasks involved in implementing the virtual memory technique in the Volume Integral Equation algorithm are twofold; the Carbrey algorithm must be extended to handle complex data and be integrated into the process of the moment method solution. Both of these difficulties have been overcome and successfully tested for small and medium scatterers. For large scatterers considerably exceeding the central memory, the computational efficiency is low and needs to be improved.

There are two steps involved in the numerical solution of a system of linear equations. First the matrix elements involved must be computed and stored for easy access. Secondly, the matrix equation must be solved by a certain process using either the central memory alone or the virtual

memory, which uses both the central memory and disk memory. Both steps need large computer execution time and the key issue is to reduce the computer time to a level acceptable for practical computations.

Figure 34 shows that the virtual memory technique requires as much as 100 times more time to generate and store the entire matrix. This poor efficiency seriously degrades the practical usefulness of the virtual memory method. However, we have discovered that by using a local file storage method the matrix storage time can be drastically reduced. This method is still being studied and will be discussed in a subsequent report.

In the numerical solution of a matrix equation, it was observed that the order and sequence of the rows and columns are incompatible between the Gauss-elimination matrix solution method and the virtual memory algorithm developed by Carbrey [45]. As a result, the direct row-access approach used by Carbrey is about ten times less efficient than the fast column-access method developed at Georgia Tech in this research program, as shown in Figure 35. However, both of them take considerably more execution time than the conventional central memory solution method.

The feasibility of the virtual memory technique in dealing with scatterers too large to be handled in computer central memory has been demonstrated. However, it is feared that the execution time may increase with the size of the scatterer so as to render the method impractical. It is hoped that the local-file manipulation method being explored can be used to improve the efficiency of the existing virtual memory technique.

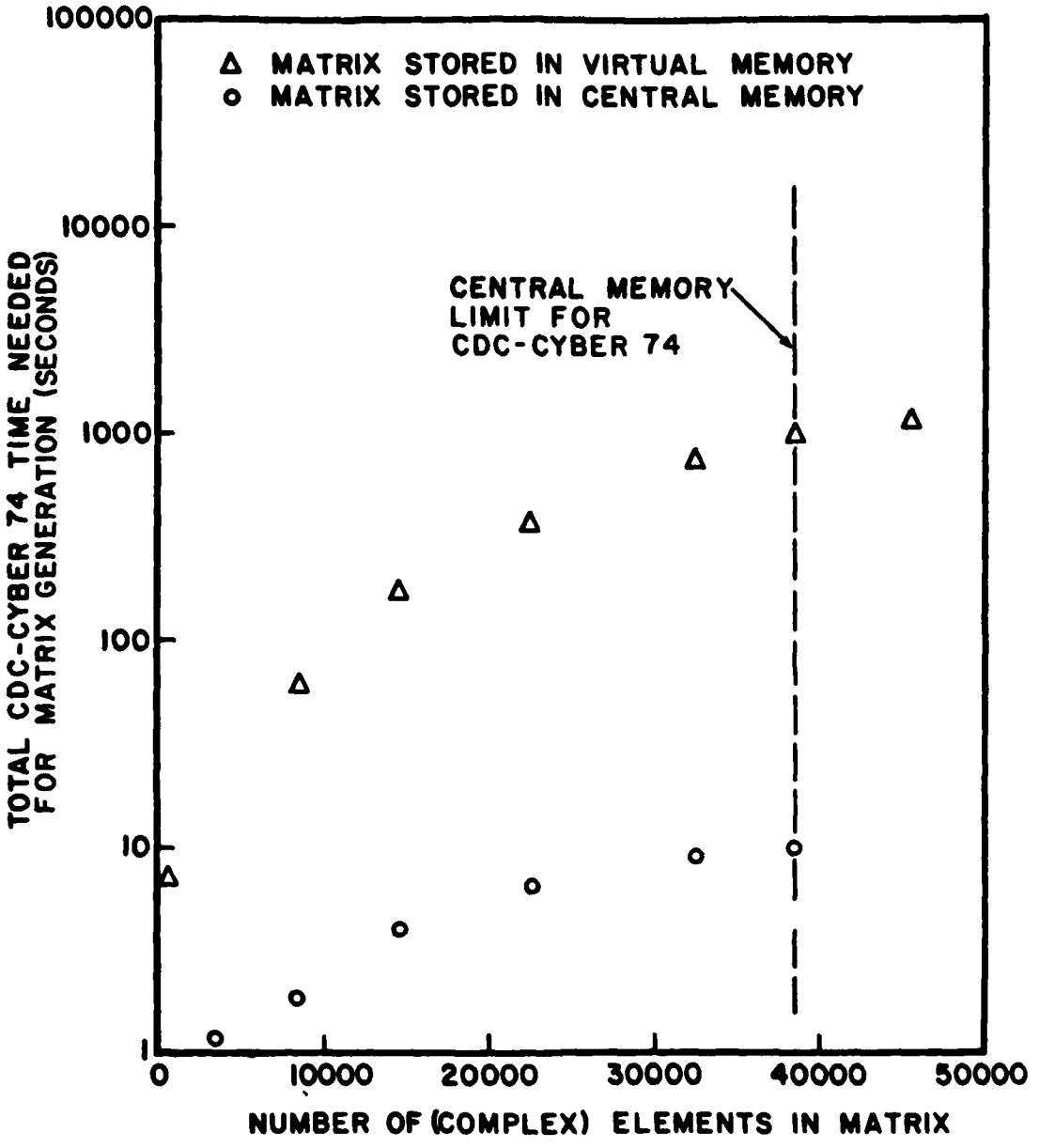

Figure 34. Comparison of computer time required to generate (including input/output time) a matrix of various sizes.

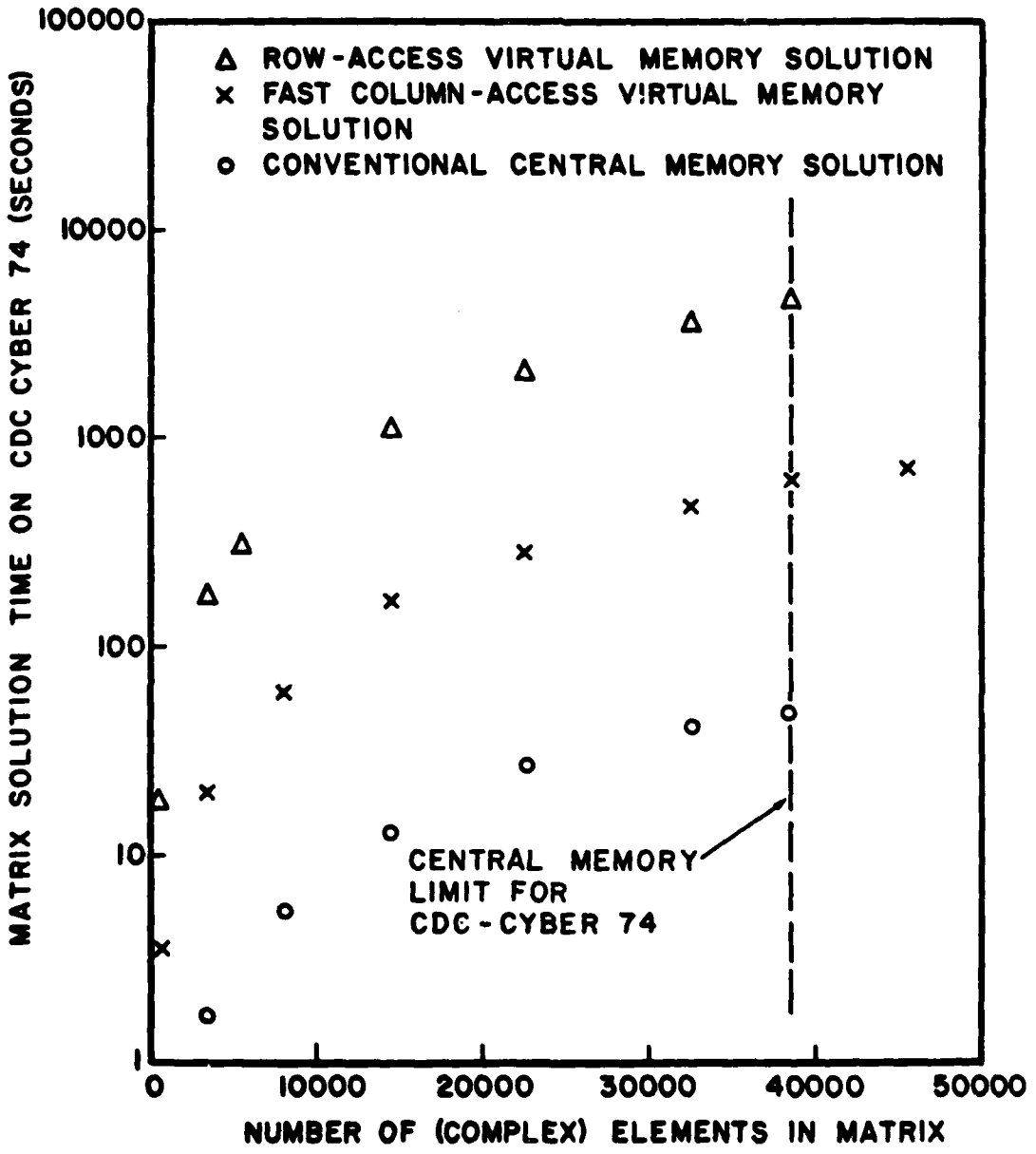

Figure 35. Comparison of matrix solution time on CDC CYBER-74 by central-memory and virtual memory techniques.

SECTION VI
CONCLUSIONS AND RECOMMENDATIONS

Research has been conducted in the analysis and measurements of three-dimensional arbitrarily-shaped heterogeneous dielectric and biological bodies. The discrepancies in the literature regarding the singularity of the electric dyadic Green's functions were resolved. The discrepancies were centered at the singularity of the rectangular cavity. It was shown in this report that the apparent discrepancies simply do not exist and were probably superficial observations.

Compact range scattering measurements were successfully conducted at 1 GHz. Techniques in fabricating simulation models using the "Super-stuff" were investigated and several 1-foot birds were made. Extensive numerical analysis was carried out for dielectric scatterers of various shapes including cylinders, rectangular blocks, I-shaped blocks, spheres, and a 1-foot bird. The accuracy of these computations was good except for the resonant sphere, for which the resonance frequencies were shifted by about 20 percent.

Various numerical techniques have been investigated. Computer central memory and execution time were reduced by 50 percent with the symmetrical matrix technique, by 75 percent for scatterers of one-plane symmetry. Techniques of banded matrix and virtual memory have been implemented in the Volume Integral Equation algorithm and tested successfully for small scatterers.

It is recommended that the area of research discussed in this report be continued except for the singularity problem associated with the electric dyadic Green's function, which appears to have been satisfactorily concluded. In addition, the Surface Integral Equation approach should be explored to see whether its numerical convergence is more rapid than the Volume Integral Equation approach. Exact solution for the dielectric prolate spheroid appears to be a feasible research subject which should lead to accurate and useful data for dielectric scattering problems.

SECTION VII

REFERENCES

1. J.J.H. Wang, "On the Dyadic Green's Functions for a Rectangular Cavity with Special Considerations to Their Application in the Source Region", 1979 IEEE International AP-S Symposium, Seattle, Washington, pp. 421-424, June 1979.

2. C. Papanicolopulos, J.J.H. Wang, E.E. Weaver, W.P. Cooke and C.E. Ryan, Jr., "Radiation and Scattering Measurements at 1 GHz Using an Indoor Compact Range", Accepted for presentation in the 1980 IEEE International AP-S Symposium, Quebec, Canada, June 1978.

3. J.J.H. Wang and C. Papanicolopulos, "Analysis of the Scattering of Arbitrarily Shaped Dielectric and Biological Bodies", Accepted for presentation in the 1980 IEEE International AP-S Symposium, Quebec, Canada.

4. C.E. Ryan, Jr., F.L. Cain, J.J.H. Wang, and B.J. Cown, "Deterministic and Statistical Models for Antenna Performance, EMC, EMI, and Biological Effects", Special Issue on Electromagnetic Modeling, IEEE Transactions on Electromagnetic Compatibility, to be published.

5. P.M. Morse and H. Feshbach, Methods of Theoretical Physics, New York: McGraw-Hill Company, 1953.

6. R.E. Collin, Field Theory of Guided Waves, New York: McGraw-Hill Company, 1960.

7. J. Schwinger and D.S. Saxon, Discontinuities in Waveguides, New York: Gordon and Breach, 1968.

8. C.T. Tai, Dyadic Green's Functions in Electromagnetic Theory, Scranton, P.A. - INTEXT, 1971.

9. R.F. Harrington, Field Computation by Moment Methods, New York: Macmillian, 1978.

10. J.A. Stratton, Electromagnetic Theory, McGraw-Hill Company, 1941.

11. C.H. Wilcox, "Debye Potentials", J. Math and Mech., Vol. 6, pp. 167-201.

12. J. Van Bladel, "Some Remarks on Green's Dyadis for Infinite Space", IRE Trans. Antennas and Propagation, Vol. AP-9, pp. 563-566, November 1961.

13. C.T. Tai, "On the Eeigen Function Expansion of Dyadic Green's Functions", Proceedings of IEEE, Vol. 61, pp. 480-481, April 1973.

AD-A089 412 GEORGIA INST OF TECH ATLANTA ENGINEERING EXPERIMENT --ETC F/G 20/3
ANALYSIS AND MEASUREMENTS OF THREE-DIMENSIONAL ARBITRARILY-SHAP--ETC(U)
MAY 80 J J WANG, C PAPANICOLOPULOS F19628-78-C-0223

UNCLASSIFIED RADC-TR-80-167 NL

2 OF 2

14. C.T. Tai and P. Rozenfeld, "Different Representations of Dyadic Green's Functions for a Rectangular Cavity", IEEE Transaction Microwave Theo. and Tech., Vol. MTT-24, pp. 597-601, September 1976.

15. R.E. Collin, "On the Incompleteness of E and H Modes in Waveguides", Canadian J. Physics, Vol. 51, pp. 1135-1140, June 1973.

16. A.Q. Howard, "On the Longitudinal Component of the Dyadic Green's Function at the Source Region in Waveguides and Cavities", Proceedings of IEEE, Vol. 62, pp. 1704-1705, December 1974.

17. Y. Rahinat-Samii, "On the Question of Computation of the Dyadic Green's Function at the Source Region in Waveguides and Cavities", IEEE Transactions Microwave Theo. and Tech., MTT-23, pp. 762-765, September 1976.

18. K.M. Chen, "A Simple Physical Picture of Tensor Green's Function in Source Region", Proceedings of IEEE, Vol. 65, pp. 1202-1204, August 1977.

19. A.D. Yaghjian, "A Direct Approach to the Derivation of Electric Dyadic Green's Functions", Digest of 1976 IEEE International Symposium on Antennas and Propagation, Anherst, MA., pp. 71-73, October 1976.

20. A.D. Yaghjian, "A Direct Approach to the Derivation of Electric Dyadic Green's Functions", NBS Technical Note 1000, January 1978.

21. A.D. Yaghjian, "Electric Dyadic Green's Functions Source Region", Proceedings of the IEEE, Vol. 68, No. 2, pp. 248-263, February 1980.

22. J.J.H. Wang, "Analysis of a Three-Dimensional Arbitrarily-Shaped Dielectric or Biological Body Inside a Rectangular Waveguide", IEEE Transactions Microwave Theo. and Tech., Vol. MTT-26, No. 7, pp. 457-462, July 1978.

23. J.W. Lee and C.L. Law, "Singularity in Green's Function and its Numerical Evaluation", Technical Report No. EM-79-10, Electromagnetic Laboratory, University of Illinois, June 1979.

24. L.B. Felsen and N. Marcavity, Radiation and Scattering of Waves, Englewood Cliffs, N.J.: Prentice Hall, Inc. 1973.

25. J.J.H. Wang, F.L. Cain, and E.C. Burdette, "Numerical Modeling of Three-Dimensional Arbitrarily-Shaped Heterogeneous Biological Bodies Under Complex Excitations", presented in the 1978 International Symposium in the Biological Effects of Electromagnetic Waves, Ottawa, Canada, June 1978.

26. D.E. Livesay and K.M. Chen, "Electromagnetic Fields Induced Inside Arbitrarily-Shaped Biological Bodies", IEEE Transactions Microwave Theo. and Tech., Vol. MTT-22, pp. 1273-1280, December 1974.

27. R.F. Harrington, Time-harmonic Electromagnetic Fields, McGraw-Hill, New York, 1961.

28. J.H. Richmond, "The Basic Theory of Harmonic Fields, Antennas and Scattering", Unpublished lecture notes, The Ohio State University, 1966.

29. R.C. Johnson, H.A. Ecker, and R.A. Moore, "Compact Range Techniques and Measurements", IEEE Trans. Ant. Prop., Vol. AP-17, No. 5, pp. 568-576, Sept. 1969.

30. D.W. Hess, F.G. Willwerth and R.C. Johnson, "Compact Range Improvements and Performance at 30 GHz", 1977 International IEEE AP-S Symposium, pp. 264-267, Stanford, Cal., June 1977.

31. R.W.P. King and T.T. Wu, The Scattering and Diffraction of Waves, Harvard University Press, Cambridge, Mass., 1957.

32. I.S. Rombauer and M.R. Becker, The Joy of Cooking, The Bobbs-Merrit Co., New York, pp. 389-424, 1953.

33. P. Blacksmith, Jr., and R.B. Mack, "On Measuring the Radar Cross Sections of Ducks and Chickens", Proceedings of IEEE, Vol. 53, p. 1125, August, 1965.

34. A.W. Guy, "Analyses of Electromagnetic Fields Induced in Biological Tissues by Thermographic Studies on Equivalent Phantom Models", IEEE Trans. Microw. Theo. Techn., Vol. MTT-19, No. 2, pp. 205-214, February 1971.

35. E.C. Burdette, F.L. Cain and J. Seals, "In-Vivo Determination of Energy Absorption in Biological Tissue", Final Technical Report, U.S. Army Grant DAAG29-75-G-0182, Engineering Experiment Station, Georgia Institute of Technology, January 1979.

36. B.S. Guru and K.M. Chen, "Experimental and Theoretical Studies on Electromagnetic Fields Induced Inside Finite Biological Bodies", IEEE Trans. Microw. Theo. Tech., Vol. MTT-24, No. 7, pp. 433-440, July 1976.

37. D.P. Nyquist, K.M. Chen and B.S. Guru, "Coupling Between Small Thin-Wire Antennas and a Biological Body", IEEE Transactions on Ant. and Prop., Vol. AP-25, No. 6, Nov. 1977.

38. M.J. Hagmann, O.P. Gandhi, and C.H. Durney, "Numerical Calculation of Electromagnetic Energy Deposition for a Realistic Model of Man", IEEE Trans. on Ant. and Prop., Vol. MTT-27, No. 9, Sept. 1979.

39. J.H. Richmond, "Digital Computer Solutions of the Rigorous Equations for Scattering Problems", Proc. IEEE, Vol. 53, pp. 796-804, August 1965.

40. D.J. Burr and Y.T. Lo, "Remote Sensing of Complex Permittivity by Multiple Resonances in RCS", IEEE Trans. Ant. Prop., Vol. AP-21, No. 4, pp. 554-561, July 1973.

41. J.J.H. Wang, "Numerical Analysis of Three-dimensional Arbitrarily-shaped Conducting Scatterers by Trilateral Surface Cell Modeling", Radio Science, Vol. 13, No. 6, pp. 947-952, Nov.-Dec., 1978.

42. J.J.H. Wang, "Study of Surface-patch Techniques for Modeling 3-D Radiating or Scattering Objects", Interim Technical Report, Contract F19628-78-C-0224, Engineering Experiment Station, Georgia Institute of Technology, Dec. 1979 (being approved for public release).

43. T. Ferguson, T.H. Lehman and R.J. Balestri, "Efficiency Solution of Large Moment Problems: Theory and Small Problem Results", IEEE Trans. Antennas Propag., Vol. AP-24, No. 2, pp. 230-235, March 1976.

44. R.J. Balestri, T.R. Ferguson and E.R. Anderson, "General Electromagnetic Model for the Analysis of Complex Systems", Technical Report RADC-TR-77-137, Vol. I and II, Rome Air Development Center (RBCT), Griffis AFB, N.Y., April 1977. Vol I A040026, Vol II A040027.

45. B.R. Carbrey, "User Manual: Virtual Memory Subroutines", Picatimny Arsenal, Dover, N.J., Transmitted to Georgia Tech, November 1977.

APPENDIX

PROOF FOR THE IDENTITIES (EQUATIONS (37-40))

Equations (37-40) were used by Tai and Rozenfeld [14] and are important identities in our proof that the expressions of Rahmat-Samii [17] and Tai and Rozenfeld [14] are identical. These four identities are similar and it suffices to prove only Equation (38).

By using an identity [R.E. Collin, Field Theory of Guided Waves, McGraw Hill, New York, 1960, p. 581]

$$\sum_{n=1}^{\infty} \frac{\mathrm{Cos}nx}{n^2-a^2} = \frac{1}{2a^2} - \frac{\pi}{2a}\,\frac{\mathrm{Cos}(\chi-\pi)a}{\mathrm{Sin}\pi a}, \quad o \le X \le 2\pi \qquad (38)$$

we can derive Equation (38) as follows

$$\sum_{\ell=1}^{\infty} \frac{1}{K^2-k^2}\ \mathrm{Cosk}_z z \mathrm{Cosk}_z z'$$

$$= \sum_{\ell=1}^{\infty} \frac{\frac{1}{2}(\frac{c}{\pi})^2}{\ell^2-[-k_x^2-k_y^2+k^2](\frac{c}{\pi})^2} \begin{Bmatrix} \mathrm{Cos}\ell\pi(z+z')/c + \mathrm{Cos}\ell\pi(z-z')/c \\ \mathrm{Cos}\ell\pi(z+z')/c + \mathrm{Cos}\ell\pi(z'-z)/c \end{Bmatrix} \text{ for } z \gtrless z'$$

$$= \frac{1}{2}(\frac{c}{\pi})^2 \begin{Bmatrix} \frac{1}{2(k_g c/\pi)^2} - \frac{\pi^2}{2k_g c} \cdot \frac{\mathrm{Cos}[(z+z')-c]k_g}{\mathrm{Sink}_g c} + \frac{1}{2(k_g c/\pi)^2} - \frac{\pi^2}{2k_g c} \cdot \frac{\mathrm{Cos}[(z-z')-c]k_g}{\mathrm{Sink}_g c} \\ \frac{1}{2(k_g c/\pi)^2} - \frac{\pi^2}{2k_g c} \cdot \frac{\mathrm{Cos}[(z+z')-c]k_g}{\mathrm{Sink}_g c} + \frac{1}{2(k_g c/\pi)^2} - \frac{\pi^2}{2k_g c} \cdot \frac{\mathrm{Cos}[(z'-z)-c]k_g}{\mathrm{Sink}_g c} \end{Bmatrix}$$

$$= \begin{Bmatrix} \frac{1}{2k_g}2 - \frac{c}{2k_g \mathrm{Sink}_g c}\ \mathrm{Cosk}_g(c-z)\mathrm{Cosk}_g z' \\ \frac{1}{2k_g}2 - \frac{c}{2k_g \mathrm{Sink}_g c}\ \mathrm{Cosk}_g(z'-c)\mathrm{Cosk}_g z \end{Bmatrix} \qquad (39)$$

Hence,

$$\sum_{\ell=0}^{\infty} \frac{\epsilon_{o\ell}}{K^2-k^2} \text{Cosk}_z z \text{Cosk}_z z' = \frac{-1}{k_g^2} + \sum_{\ell=1}^{\infty} \frac{2}{K^2-k^2} \text{Cosk}_z z \text{Cosk}_z z' \qquad (40)$$

$$= -\frac{c}{k_g \text{Sink}_g c} \begin{cases} \text{Cosk}_g(z-c)\text{Cosk}_g z' \\ \text{Cosk}_g(z'-c)\text{Cosk}_g z \end{cases} \quad z \gtrless z' \; .$$

This completes the proof for Equation (38). Similarly, Equations (37), (38) and (40) can be proved by using the series summations in Collin's book and the combination of sinusoidal functions.

★ U.S. GOVERNMENT PRINTING OFFICE: 1980--600-039--7

MISSION
of
Rome Air Development Center

RADC plans and executes research, development, test and selected acquisition programs in support of Command, Control Communications and Intelligence (C^3I) activities. Technical and engineering support within areas of technical competence is provided to ESD Program Offices (POs) and other ESD elements. The principal technical mission areas are communications, electromagnetic guidance and control, surveillance of ground and aerospace objects, intelligence data collection and handling, information system technology, ionospheric propagation, solid state sciences, microwave physics and electronic reliability, maintainability and compatibility.